1. SUMMARY

Three-phase fluidized beds are expected to have increasing application in coal liquefaction and gasification. An investigation of fluidization and mass transfer in a cocurrent three-phase fluidized bed has been initiated by the Chemical Technology Division at ORNL.

The experimental apparatus consisted of a 3-in.-diam column with water and air-carbon dioxide feed lines. Four packings were used to study changes in fluidization and mass transfer due to size, shape, and density. Pressure drop and volume fractions of the three phases were measured for a number of liquid flow rates for each of four gas flow rates. Incipient fluidization was determined from a plot of pressure drop versus liquid flow rate as the point where the pressure drop dependence on liquid flow rate is ended. Quantitative correlations of incipient fluidization and volume fraction for each phase to the flow rates were investigated. The solid volume fraction has the following correlation with the liquid velocity:

$$\epsilon_S = 0.51\left(\frac{U_L}{U_{L_{mf}}}\right)^{-0.076\pm0.02}$$

The remaining data were scattered due to experimental error and could not be correlated. Several experimental improvements are suggested.

Concentration profiles were measured experimentally by sampling the liquid phase at five heights in the column, and the best dispersion coefficient for a backmixing model for each experimental run was determined. Alumina beads produced plug flow fluidization and a higher mass transfer coefficient, while the Plexiglas beads produced a column with a higher dispersion coefficient and a lower mass transfer coefficient than a bubble column at comparable flow rates.

2. INTRODUCTION

2.1 Background

Three-phase fluidized beds, consisting of solid particles fluidized by gas and liquid flows, are expected to be applied in coal liquefaction and gasification processes. The three-phase fluidized bed would consist of solid catalyst particles, a liquid slurry of pulverized coal in a coal-derived oil, and hydrogen gas. Three-phase fluidized beds are currently used for the catalytic hydrogenation of liquid petroleum fractions. A program to determine the operating characteristics of a three-phase fluidized bed has been started by the Chemical Technology Division of ORNL.

2.2 Previous Work

A previous MIT group (1) has investigated operat'ng charac istics and mass transfer in the three-phase fluidized bed. The requi: liquid velocity for minimum fluidization and the pressure drop acros flui- dized bed decreased as the gas velocity increased. Increasi er'icial gas velocity increased the gas volume fraction and decreased olid volume fraction. Increasing superficial liquid velocity de the overall gas and solid volume fractions. Mass transfer in dized bed with 4x8 mesh alumina was closely approximated by a plug flow model. The overall mass transfer coefficients which were found are presented in Table 1.

Table 1. Previous Mass Transfer Results (1)

$K_L a_{pf}$ (sec^{-1})	U_G (cm/sec)	U_L (cm/sec)
0.018	10.4	3.[illegible]
0.072	10.6	5.5
0.10	10.4	5.5

Michelson and Ostergaard (2) reported the relation of the dispersion and mass transfer coefficients in three phase fluidized beds to liquid flow rate for particles of several sizes and a density of 2.6 gm/cc. Particles of 6-mm diameter were found to increase the mass transfer coefficient compared to a bubble column, while 1-mm particles decreased it. The dispersion coefficient increased with liquid flow rate and decreased with liquid volume fraction, which is a function of the gas flow rate.

2.3 Objectives

The objectives were: (1) to propose a method for determining the liquid volume fraction independently of the gas and solid volume fractions, (2) to investigate further the effect on fluidization of the following hydrodynamic variables - column pressure drop, gas and liquid fluidization velocities, and the volume fractions of the three phases, (3) to determine overall mass transfer coefficients for two packings and an open bubble column, and (4) to correlate hydrodynamic variables and overall mass transfer coefficients with those reported previously.

2.4 Method of Approach

The effect of hydrodynamic variables on fluidization was studied using a 3-in.-diam Plexiglas column. Four packings (4x8 and 8x12 mesh alumina beads, 0.25-in. Plexiglas spheres, and 3/32-in. Plexiglas cubes), varying in size, shape, and density were fluidized by a range of gas and liquid superficial velocities spanning the region of incipient fluidization. The volume fractions of the three phases in the three-phase region of the column were recorded. Correlations of the data with a least squares computer program were attempted.

The absorption of carbon dioxide gas into the liquid phase was studied at a relatively constant extraction factor, F,

$$F = \frac{mU_L}{U_G} \tag{1}$$

for flow velocities in the fluidized range. With the experimental flow data and carbon dioxide concentration measurements, computer programs were used to calculate the best dispersion coefficient and overall mass transfer coefficient for the experimental concentration profile in the column. The results of the mass transfer experiments were then compared to find the dependence of the calculated coefficients on packing density and the degree of fluidization.

3. APPARATUS AND PROCEDURE

3.1 Apparatus

The three-phase fluidized bed operated in a 3-in.-diam x 5-ft-long Plexiglas column which was equipped with a sight tube to measure the pressure drop through the column. Sample ports were located approximately every 10 cm up the column. A diagram of the 3-in.-diam column is shown in Fig. 1.

Water from two feed tanks entered the column bottom after passing through a rotameter. A 50-mesh screen above the liquid inlet distributed the liquid evenly across the column. Air and carbon dioxide were passed through separate rotameters before mixing in a surge tank. The gas stream entered the column through a distributor located 1.5-in. above the liquid screen distributor. Liquid overflowed from the column top through a screen into a 1-in.-diam hose to either the drain or the top of a 6-in.-diam Plexiglas column. The liquid drained from the 6-in. column into a feed tank. The 6-in. column contained 0.25-in. Raschig rings and 3/32-in. Plexiglas cubes. Air could be passed through the column countercurrent to the liquid to operate the column as a carbon dioxide stripper. A diagram of the entire apparatus is shown in Fig. 2.

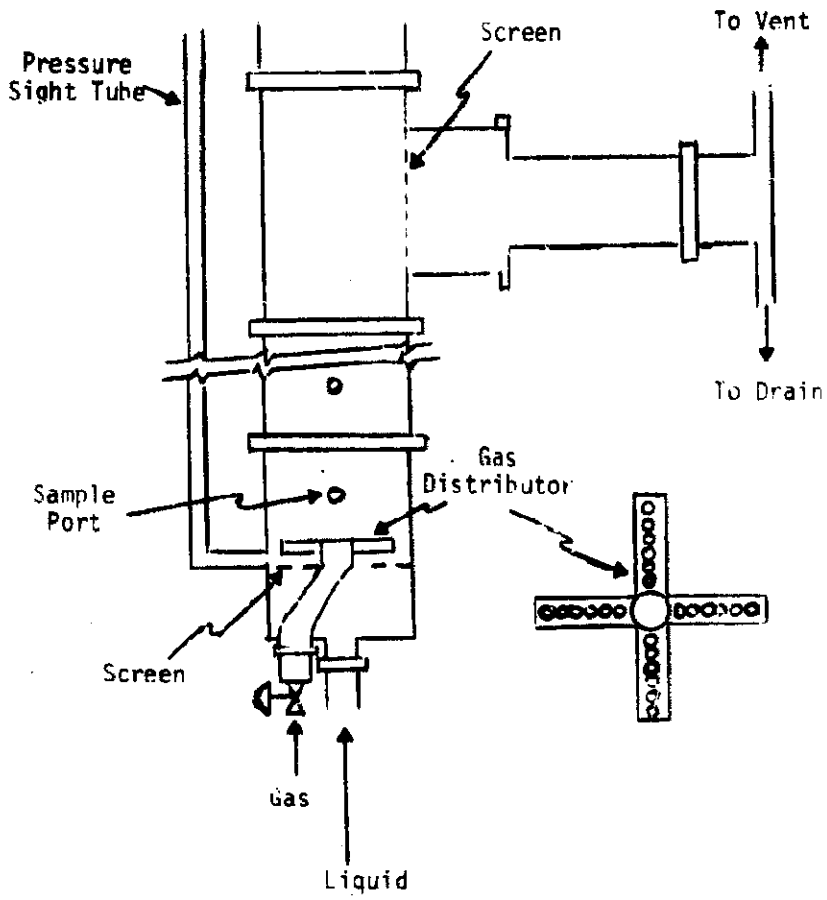

MASSACHUSETTS INSTITUTE OF TECHNOLOGY
SCHOOL OF CHEMICAL ENGINEERING PRACTICE
AT
OAK RIDGE NATIONAL LABORATORY

DIAGRAM OF 3-in.-DIAM COLUMN

DATE	DRAWN BY	FILE NO.	FIG.
5-19-75	RM	CEPS-X-213	1

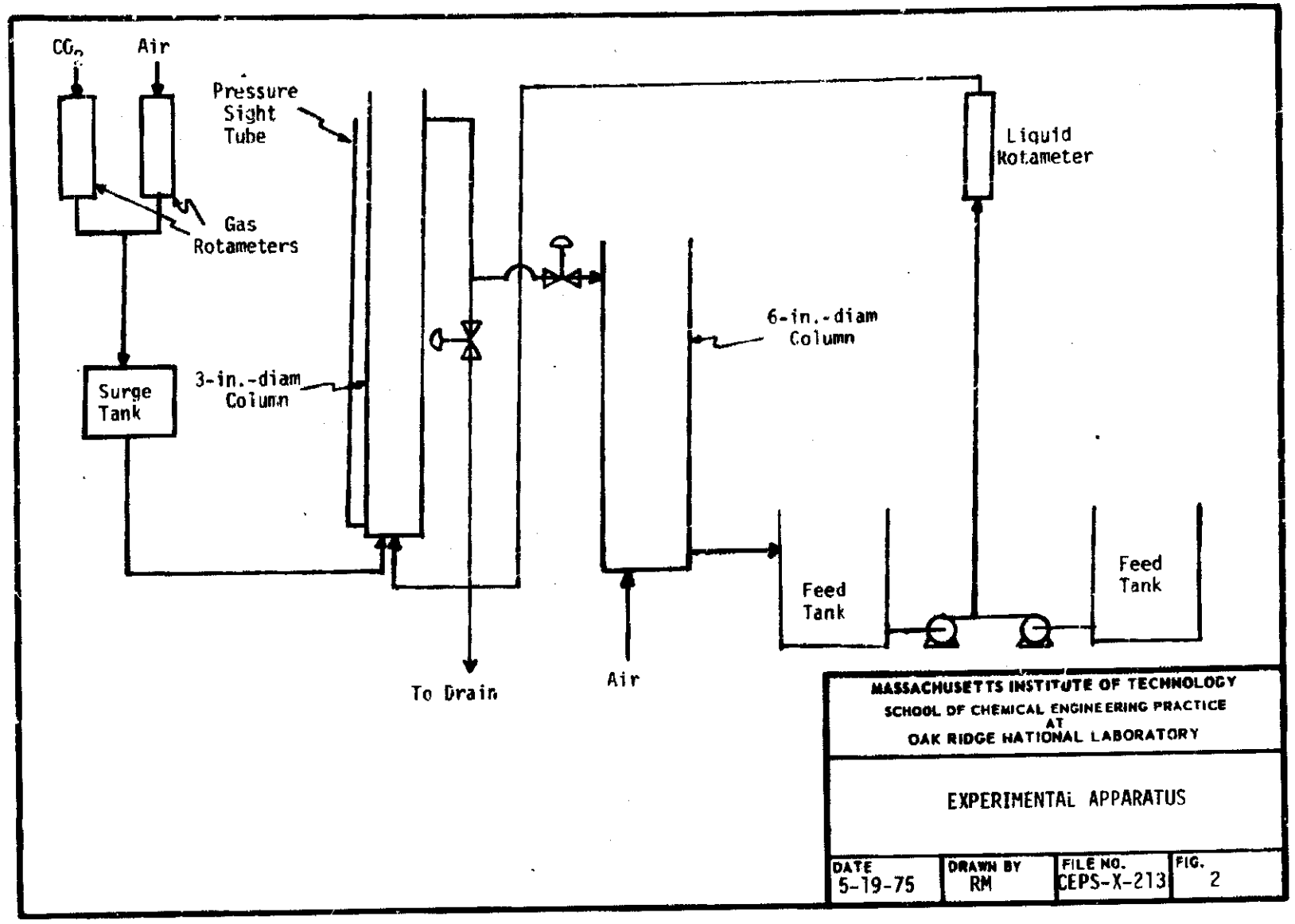
CO_2
Air
Pressure Sight Tube
Gas Rotameters
Surge Tank
3-in.-diam Column
To Drain
6-in.-diam Column
Air
Liquid Rotameter
Feed Tank
Feed Tank
MASSACHUSETTS INSTITUTE OF TECHNOLOGY
SCHOOL OF CHEMICAL ENGINEERING PRACTICE
AT
OAK RIDGE NATIONAL LABORATORY
EXPERIMENTAL APPARATUS
DATE 5-19-75
DRAWN BY RM
FILE NO. CEPS-X-213
FIG. 2

The previous MIT group had difficulty maintaining a stable liquid level above the drain outlet. To maintain the liquid level above the column outlet, the drain hose was initially elevated on a metal support. At high flow rates, the hose filled completely with water, siphoning the liquid level down to the column outlet. This broke the siphon and the liquid level then increased until the height of the top of the hose was reached. Again the siphon formed, lowering the level. The instability in the liquid level was corrected by installing a vent at the maximum height of the drain line which prevented siphon formation.

3.2 Hydrodynamic Experimental Procedure

The fluidization behavior of four packings (4x8 mesh and 8x12 mesh activated alumina beads, 3/32-in. Plexiglas cubes and 0.25-in. Plexiglas spheres) distinct in size, density, or shape was studied in a cocurrent three-phase fluidized bed as a function of superficial liquid and gas velocities. The volume fraction of each phase was determined as a function of the superficial gas and liquid velocities as well as the size, density, and shape of the solid particles.

For each of the five superficial gas velocities ranging from 0 to 3.5 cm/sec, the liquid superficial velocity was varied approximately $\pm 75\%$ from incipient fluidization. The operating conditions for the experiments are summarized in Table 2.

The pressure drop through the column was measured by comparing the liquid height in the column to that in a parallel sight tube. This difference was corrected for the pressure drop of the bubble column region.

Experiments for each packing, except the 3/32-in. Plexiglas cubes, were run with two different static bed heights in the column. The average gas volume fraction for each column was found by stopping all fluid flows simultaneously and measuring the drop in the liquid level. The gas volume fraction in both the three-phase region and the bubble column was assumed to be independent of static bed heights. The gas volume fraction for each region could be determined by solving the simultaneous equations derived for the two columns (see Appendix 8.3). The solid volume fraction was calculated from:

$$\varepsilon_S = \frac{W}{\rho_S A H} \tag{2}$$

The liquid volume fraction was determined from:

$$\varepsilon_L = 1 - \varepsilon_S - \varepsilon_G \tag{3}$$

Procedural details are presented in Appendix 8.1.

Table 2. Operating Conditions for Hydrodynamic Experiments

Run No.	Packing Material	Size of Packing	ρ_S (gm/cm^3)	Lower Bed Height, h_{11} (cm)	Higher Bed Height, h_{21} (cm)	U_L (cm/sec)	U_G (cm/sec)
II	alumina	8x12 mesh spheres (0.21 cm OD)	1.63	22	55	0 - 4.1	0 0.57 1.51 2.47 3.51
III	none (bubble column)	-	-	40.2 65.7 87.2 121.7	-	-	0.57 1.51 2.47 3.51
IV	alumina	4x8 mesh spheres (0.64 cm OD)	1.93	22	40	0 - 7.48	0 0.57 1.51 2.47 3.51
V	Plexiglas	3/32 in. (edge) cubes	1.17	34	-	0 - 5.0	0.28 0.57 1.17 1.75
VI	Plexiglas	0.25 in. spheres (0.64 cm OD)	1.17	26	50	0 - 5.0	0 0.57 1.51 2.47 3.51

3.3 Mass Transfer Experimental Procedure

Overall mass transfer coefficients for the absorption of carbon dioxide into water were determined for an open bubble column and for a fluidized bed with two packings of different densities: 0.25-in. Plexiglas spheres and 4x8 mesh alumina beads. The choice of flow rates in the fluidizing region was constrained to a constant extraction factor of less than 0.6, which minimizes error in the computation of the overall mass transfer coefficient (1).

Each packing was operated at and above incipient fluidization conditions. Incipient fluidization conditions for the alumina were used for one Plexiglas run as a comparison. The Plexiglas flow conditions were used again for the bubble column runs to provide another comparison. These conditions are later summarized (see Table 5 in Sect. 4.2).

The initial carbon dioxide concentration in the air flow was determined from the separate gas flow rates. Absorption was monitored by titrating samples from a sample port with an automatic titrator until steady state was reached. Then four samples from each of the column sample ports were titrated and the results were averaged. The water flow was stopped, and the liquid became saturated with carbon dioxide. The value of Henry's Law constant was then found from the liquid carbon dioxide concentration. Procedural details are presented in Appendix 8.2.

With the flow and titration data, a computer program TPFBED was used to calculate the concentration profile and the overall mass transfer coefficient; plug flow behavior was assumed for both phases (see Appendix 8.6). Computer programs TPFBED and BLE were then used to calculate the overall mass transfer coefficient for a plug flow gas and dispersed liquid model. The dispersion coefficient was varied to obtain the best fit of the predicted concentration profile to the experimental profile. The overall mass transfer coefficient was also calculated for a gas phase in plug flow with an ideally well-mixed liquid phase (CSTR model). The equations relating concentration and the overall mass transfer coefficient for the models are shown in Table 3. Overall mass transfer coefficients were correlated with hydrodynamic and flow variables. A description of the computer programs used to analyze the data is found in Appendix 8.6.

4. RESULTS AND DISCUSSION

4.1 Hydrodynamics

The forces acting on a fluidized bed are an upward drag force, ΔPA, and the downward buoyant weight of the particles, W_b, in the medium. At the point of fluidization, these forces are equal:

Table 3. Dimensionless Concentration for Various Mixing Models (1)

1. For a model in which there is no axial mixing in gas or liquid phases:

$$X = \frac{F + e^{-[(F+1)(K_L a\ h)]/U_L}}{F + 1} \tag{4}$$

2. For a model in which there is no axial mixing in the gas phase and in which the axial mixing in the liquid phase is characterized by a finite dispersion coefficient:

$$X = 1 - \left(\frac{1}{F+1}\right) + \frac{1}{F+1}\left[\frac{\dfrac{e^{\mu_2 Z}}{\mu_2 e^{\mu_2}} - \dfrac{e^{\mu_1 Z}}{\mu_1 e^{\mu_1}}}{\dfrac{1 - \dfrac{E_L \mu_2}{U_L h}}{\mu_2 e^{\mu_2}} - \dfrac{1 - \dfrac{E_L \mu_1}{U_L h}}{\mu_1 e^{\mu_1}}}\right] \tag{5}$$

where:

$$\mu_{1,2} = \frac{-\left[\frac{E(NTU)}{U_L H} - \frac{1}{F}\right] \pm \sqrt{\left[\frac{E(NTU)}{U_L H} - \frac{1}{F}\right]^2 + \frac{4E}{FU_L H}\left(NTU + \frac{1}{F} + 1\right)}}{2E/FU_L H} \tag{6}$$

$\mu_2 < \mu_1$

NTU is varied until $X_{calculated} = X_{experimental}$.

3. For a model in which there is no axial mixing in the gas phase and the axial mixing in the liquid phase is characterized by an infinite dispersion coefficient:

$$X = \frac{F}{1 + F - e^{-FK_L ah/U_L}} \tag{7}$$

$$\Delta PA = W_b = (1 - \epsilon_{ns})(\rho_S - \rho_{ns})HA \tag{8}$$

Equation (8) can be rearranged to give:

$$\left(\frac{\Delta P}{W_b/A}\right)_{\text{at incipient fluidization}} = \frac{\Delta P}{\epsilon_S(\rho_S - \rho_{ns})H} = 1.0 \tag{9}$$

The ratio of the drag force to the weight is interpreted as a fractional approach to fluidization.

Typical curves of the nondimensional pressure drop, $\Delta P/(W_b/A)$, as a function of the flow rates for 4x8 mesh alumina beads are shown in Fig. 3. The pressure drop through the three-phase region was calculated by subtracting the bubble column contribution to pressure drop from the total column pressure drop. The buoyant weight of particles in the static liquid was used in the weight per unit area term. The force ratio in the fluidized bed region does not reach a value of one for the curves with higher gas flow rates.

The gas fraction is incorporated into the force ratio by replacing the liquid (or non-solid) phase density with an appropriate term:

$$\frac{\Delta P}{W_b/A} = \frac{\Delta P}{\epsilon_S[\rho_S - (\epsilon_G'\rho_G + \epsilon_L'\rho_L)]H} \tag{10}$$

where:

$$\epsilon_G' = \frac{\epsilon_G}{\epsilon_G + \epsilon_L}, \text{ normalized gas volume fraction}$$

$$\epsilon_L' = \frac{\epsilon_L}{\epsilon_G + \epsilon_L}, \text{ normalized liquid volume fraction}$$

The non-solid density is now a function of the gas and liquid volume fractions and densities. The modified equation should result in curves with a dimensionless pressure drop equal to one in the fluidized region within experimental error. A correlation of the non-solid volume fraction with the operating variables (e.g., the superficial gas and liquid velocities, and packing size, shape, and density) enables a direct correlation of fluidization to these variables.

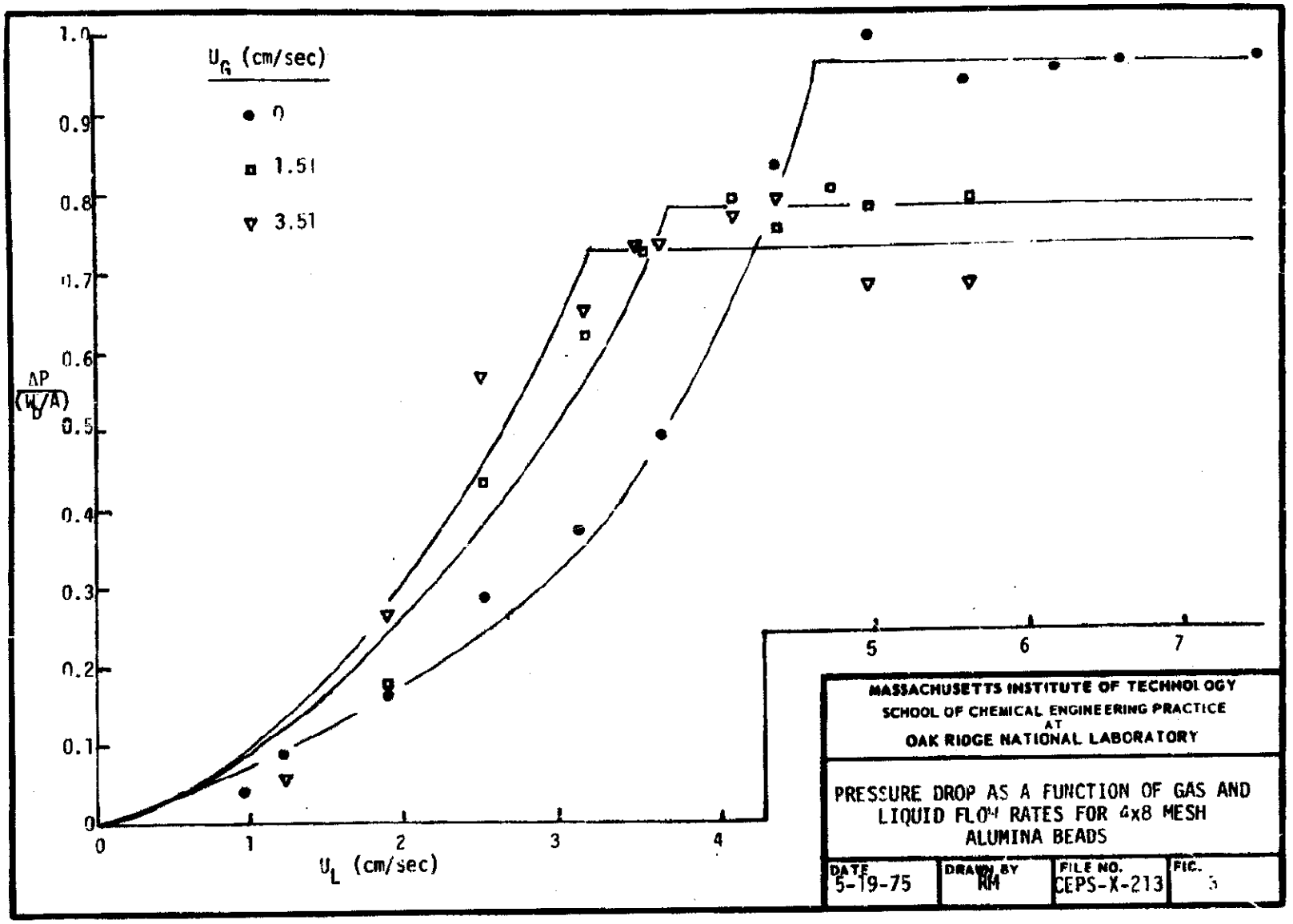

MASSACHUSETTS INSTITUTE OF TECHNOLOGY
SCHOOL OF CHEMICAL ENGINEERING PRACTICE
AT
OAK RIDGE NATIONAL LABORATORY

PRESSURE DROP AS A FUNCTION OF GAS AND LIQUID FLOW RATES FOR 4x8 MESH ALUMINA BEADS

DATE	DRAWN BY	FILE NO.	FIG.
5-19-75	RM	CEPS-X-213	3

4.1.1 Effect of Flow Rates on Pressure Drop

Two flow regimes occurred in each run: the packed bed regime in which the force ratio is a linear function of superficial liquid velocity at a constant superficial gas velocity and the fluidized regime where the pressure drop is independent of the liquid flow rate. The only parameter varying with the force ratio is the pressure drop. Thus, the curvature in the packed bed region is due to a linear function between the pressure drop and the superficial liquid velocity. The flow velocities at the intersection of the packed bed and the fluidized bed curves are called the incipient fluidization velocities. At this point the packed bed arrangement is disrupted and the bed begins to expand. At higher liquid velocities the non-solid volume fraction is increased, resulting in decreasing resistance to flow and a constant pressure drop.

The curves in Fig. 3 shift leftward and downward with increasing superficial gas velocity. For a constant liquid velocity in the fluidization region, as gas velocity increases, the void fraction increases, resulting in a lower pressure drop. Similarly in the packed bed region, at a constant liquid velocity, the increase in gas velocity decreases the space through which liquid flows. The pressure drop increases and the fluidization occurs at a lower liquid velocity.

4.1.2 Relation of Gas and Liquid Velocities at Incipient Fluidization

The relation between gas and liquid velocities at incipient fluidization is illustrated in Fig. 4. A lower liquid velocity is required for smaller particles to reach incipient fluidization for a constant gas velocity. For a given gas velocity and packing, as the bed height is increased, the incipient liquid fluidization velocity decreased in most cases. At some liquid velocity, characteristic of the packing, the incipient fluidization point becomes nearly independent of gas velocity. A gas-solid bed of 0.25-in. alumina spheres is predicted to fluidize at a superficial gas velocity of approximately 200 cm/sec (1), which is above the gas velocities of 0 to 4 cm/sec observed in Fig. 4.

The gas distributor located 3.8 cm above the liquid distributor may cause an end effect or a region in the lower part of the column which is fluidized only by liquid. As the gas velocity increases for a very low bed height (~3.8 cm), the incipient liquid fluidization velocity should remain constant. As the bed height increases, the importance of this end effect should decrease. To test this hypothesis, experiments should be conducted for different heights of packing in a column where the liquid and gas distributors are on the same plane. If the incipient fluidization velocities are independent of height, the end effect hypothesis is correct.

4.1.3 Effect of Flow Rates and Bed Height on Solid Volume Fraction

In Fig. 5 the solid volume fraction of 4x8 mesh alumina is plotted as a function of the superficial gas and liquid velocities and the bed height. The packed bed and fluidized bed regions are distinct. The solid volume fraction remains constant at 0.6 as liquid velocity increases from

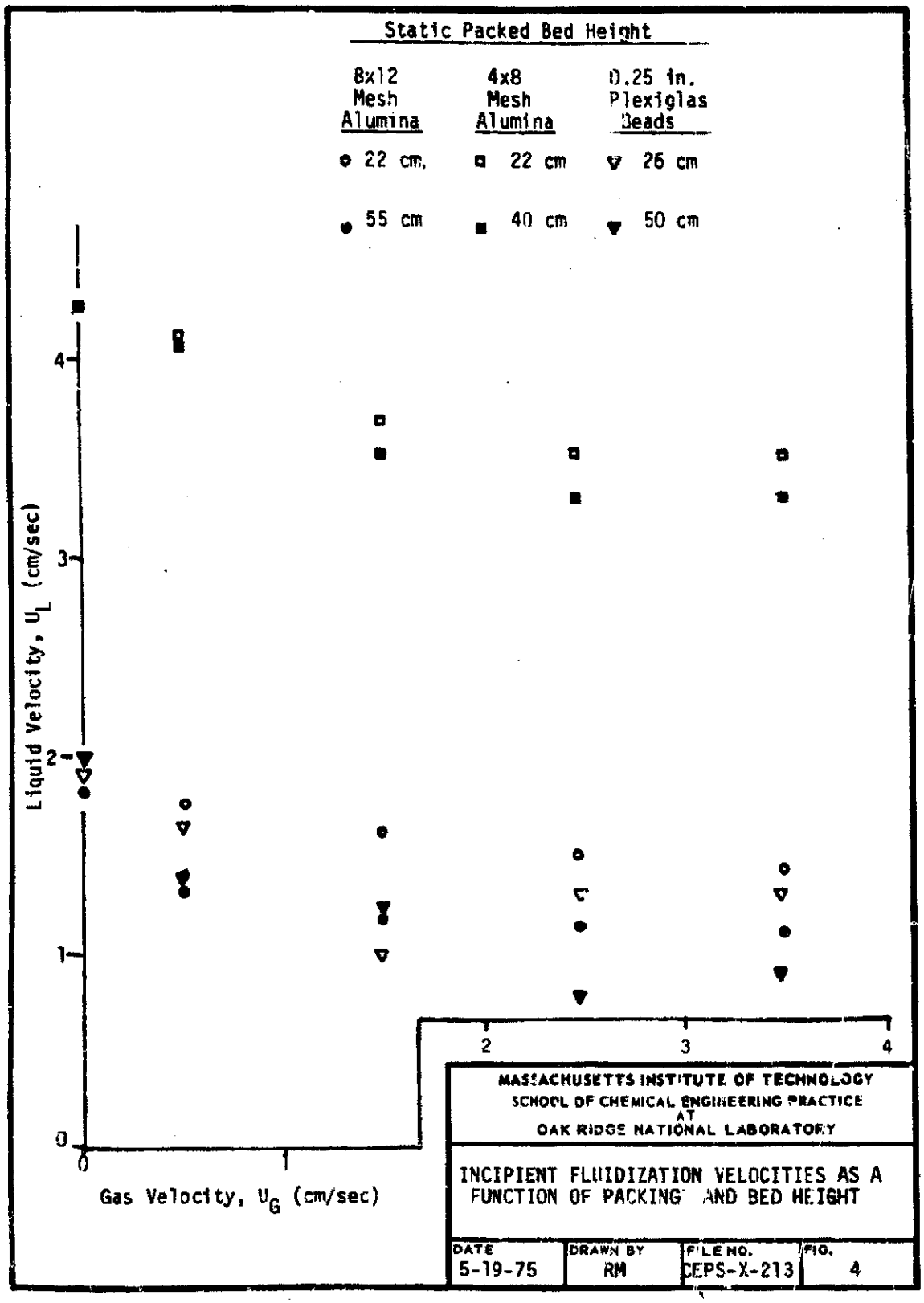
Static Packed Bed Height
8x12 Mesh Alumina
4x8 Mesh Alumina
0.25 in. Plexiglas Beads
22 cm
55 cm
22 cm
40 cm
26 cm
50 cm
Liquid Velocity, U_L (cm/sec)
Gas Velocity, U_G (cm/sec)
0
1
2
3
4
MASSACHUSETTS INSTITUTE OF TECHNOLOGY
SCHOOL OF CHEMICAL ENGINEERING PRACTICE
AT
OAK RIDGE NATIONAL LABORATORY
INCIPIENT FLUIDIZATION VELOCITIES AS A FUNCTION OF PACKING AND BED HEIGHT
DATE 5-19-75
DRAWN BY RM
FILE NO. CEPS-X-213
FIG. 4

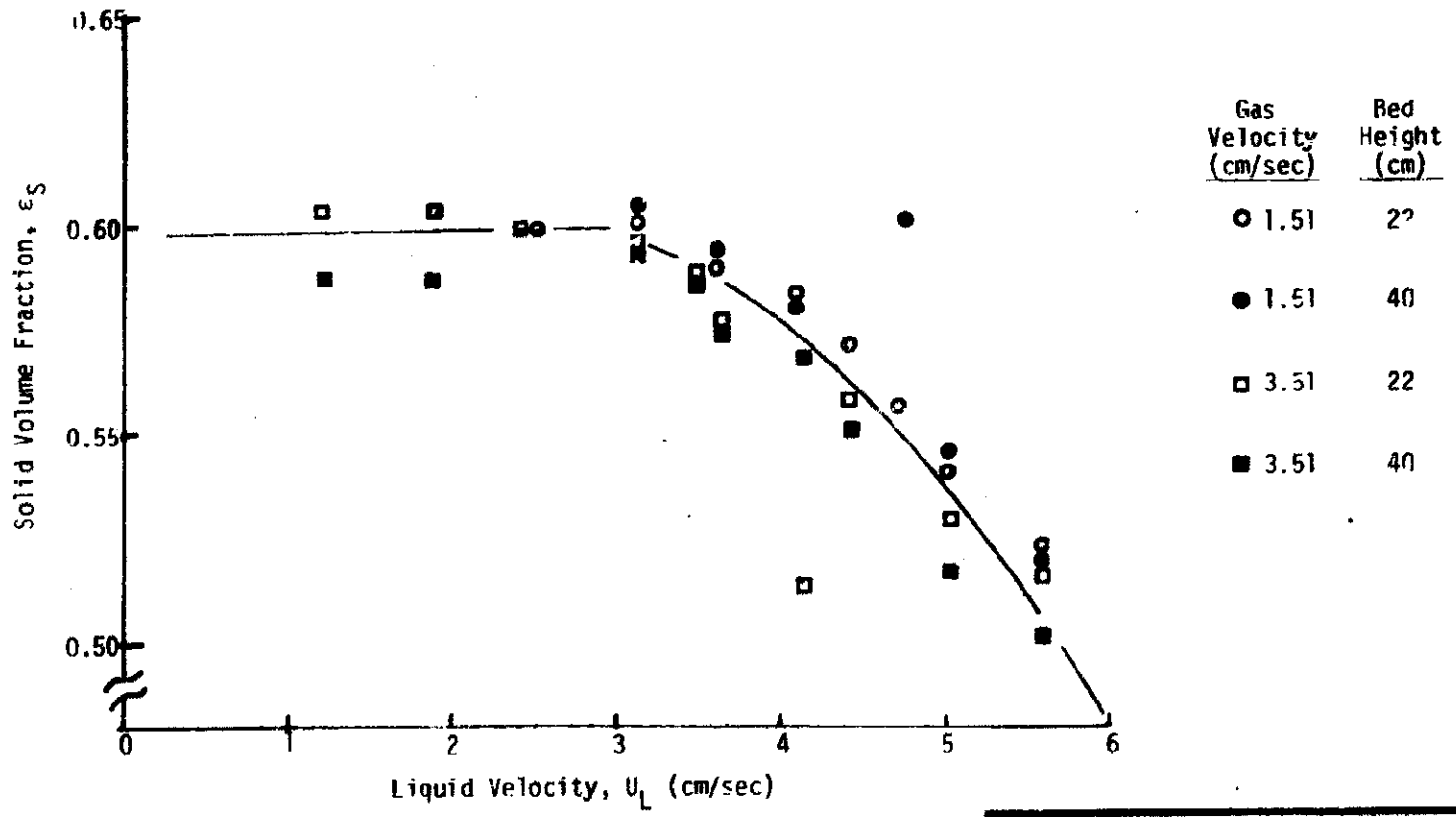

MASSACHUSETTS INSTITUTE OF TECHNOLOGY
SCHOOL OF CHEMICAL ENGINEERING PRACTICE
AT
OAK RIDGE NATIONAL LABORATORY

EFFECT OF GAS AND LIQUID VELOCITIES ON SOLID VOLUME FRACTION OF 4x6 MESH ALUMINA

DATE	DRAWN BY	FILE NO.	FIG.
5-19-75	RM	CEPS-X-213	5

0 to ∿3 cm/sec and then begins to decline. In the force ratio and superficial liquid velocity correlation, the pressure drop increases with higher liquid velocity while the bed height remains constant. Then the bed expands and the pressure drop remains constant. The change in the slope for the solid volume fraction at about 3 cm/sec corresponds closely to the onset of fluidization predicted by the incipient fluidization velocities correlation. The solid volume fraction is essentially independent of superficial gas velocity and bed height.

4.1.4 Effect of Flow Rates on Gas Volume Fraction

In Fig. 6 the gas volume fraction in the three-phase 4x8 mesh alumina bed is plotted as a function of the superficial liquid and gas velocities. Since the data are scattered, further work is necessary to eliminate the possible sources of error in the gas volume fraction determination. The errors that occur in measuring the various heights and flows should be minimized. A method for removing the gas that is retained in the bed after the gas flow has been shut off should be developed. Finally, liquid flowing into and out of the column could not be halted exactly at the same moment; a ball valve installed in the exit line at the column outlet would be a major improvement. A least-squares fit to the data produced no statistically significant results.

4.1.5 Effect of Packing Characteristics on Volume Fractions

The volume fraction for each phase was investigated as a function of size, density, and shape factor. The particle size is represented by its diameter. The shape factor is the ratio of the surface area of a spherical particle having the same volume of the particle to the area of the particle.

The effect of diameter on volume fractions for constant density, shape, bed height, and flow rates was studied by comparing the 4x8 and 8x12 mesh alumina beads. Qualitatively, as diameter increased, both liquid and gas volume fractions in the three-phase region increased while the solid volume fraction decreased.

The effect of particle density on volume fractions was investigated by comparing 0.25-in. alumina and Plexiglas spheres while the other parameters remained constant. As density increased, the gas and solid volume fractions increased while the liquid volume fraction decreased.

The effect of particle shape on volume fraction using two packings, 3/32-in. Plexiglas cubes with a shape factor of 0.81 and 0.25-in. Plexiglas spheres with a shape factor of 1.0, was investigated. The nonwetting action of grooves on the cubes caused a large portion of the cubes to remain at the top of the column since small air bubbles were attached to the cubes. Consequently, the bed was not uniformly fluidized and the data for this packing were uncertain, so no qualitative correlations could be made.

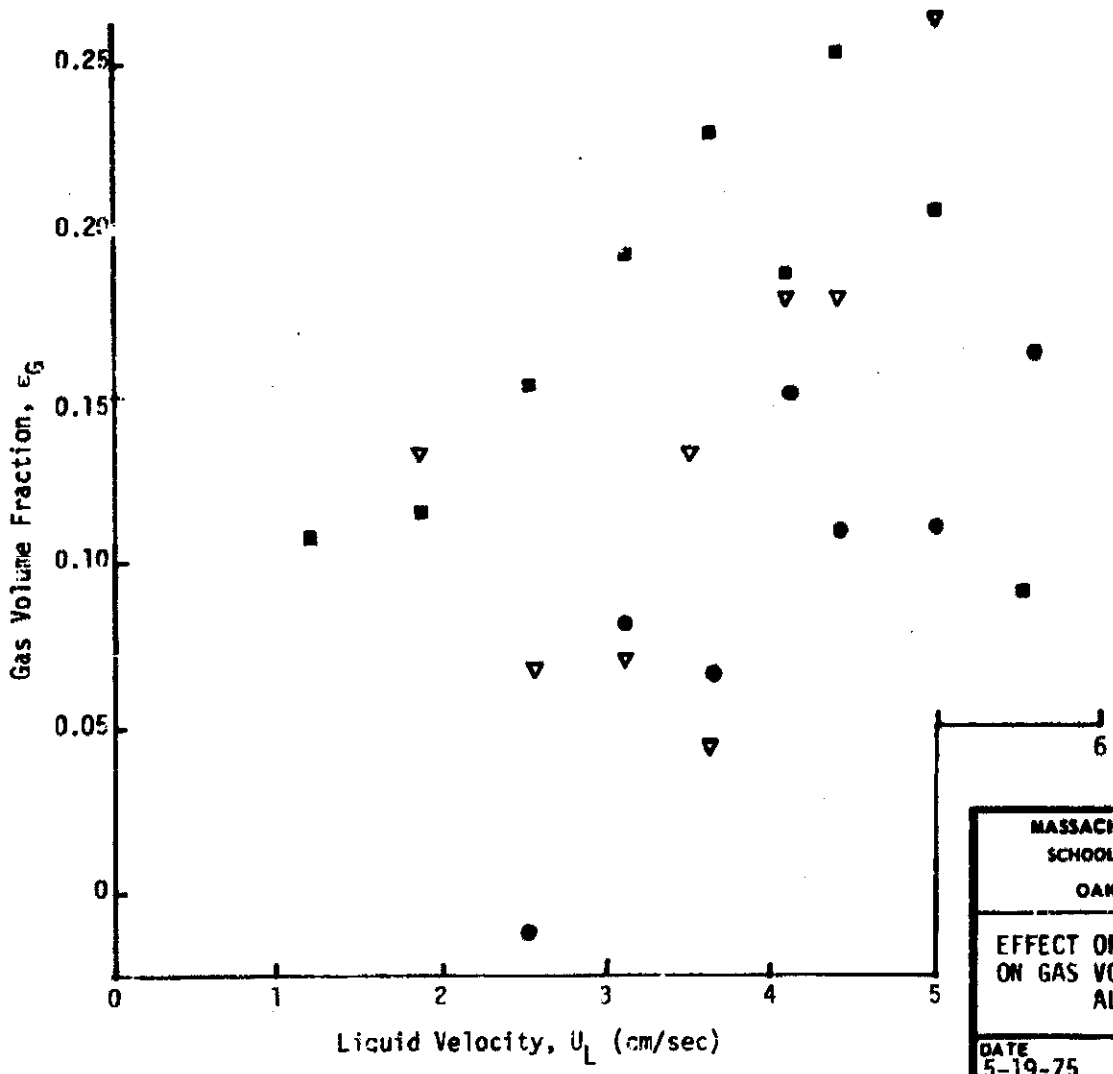

MASSACHUSETTS INSTITUTE OF TECHNOLOGY
SCHOOL OF CHEMICAL ENGINEERING PRACTICE
AT
OAK RIDGE NATIONAL LABORATORY

EFFECT OF GAS AND LIQUID VELOCITIES ON GAS VOLUME FRACTION IN 4x8 MESH ALUMINA FLUIDIZED BED

DATE	DRAWN BY	FILE NO.	FIG.
5-19-75	GM	CEPS-X-21	6

4.1.6 Multiple Linear Regression for the Solid Volume Fraction Correlation

Only the data for the solid volume fraction and incipient fluidization are sufficiently consistent to be correlated quantitatively as a function of the superficial gas and liquid velocities. The superficial velocities and solid volume fraction were related to the minimum fluidization velocities. Two empirical relations were considered:

$$\left(\frac{U_{G_{mf}}}{U^{o}_{G_{mf}}}\right) = a\left(\frac{U_{L_{mf}}}{U^{o}_{L_{mf}}}\right)^{b} \tag{11}$$

and

$$\epsilon_S = a\left(\frac{U_L}{U_{L_{mf}}}\right)^{b}(U_G)^{c} \tag{12}$$

As shown in Fig. 5 the solid volume fraction decreases with increasing liquid velocity in the fluidized region, but was independent of flow in the packed bed region. Thus, a correlation was derived for the fluidized region alone.

For Eq. (11) the minimum fluidization liquid velocity at zero gas velocity was determined experimentally by eliminating the gas flow. Since the gas velocity required to fluidize the solid bed for a gas-solid system was beyond the capability of the present apparatus, the minimum gas fluidization velocity at zero liquid flow was calculated by applying the Blake-Plummer variation for turbulent flow of the Ergun Equation (see Appendix B.3.4). These minimum fluidization flow rates were used to normalize the three-phase incipient fluidization velocities. Equations (11) and (12) were applied separately to each of the three packings. Additionally, the solid volume fraction correlation was applied to data for all packings, making the correlation independent of packing characteristics. The summary of the results using the multiple linear regression program, MLR2, is shown in Table 4.

The multiple correlation coefficient and the F-value for the regressions are listed in Table 4. A correlation coefficient is a measure of the degree of relation among variables. A correlation coefficient of 1.0 indicates a perfect relation among the variables; a correlation coefficient of 0.0 indicates a completely random relation. The F-value is a test for the significance of the multiple regression. Generally, as the F-value increases the correlation becomes better.

Lower correlation coefficients were found for the minimum fluidization velocity regressions in comparison to the solid volume fraction correlations probably because the greater dependence of the minimum fluidization velocities on bed height was neglected in the empirical relations. None of the minimum fluidization velocity relations, having greater standard deviations than the regression coefficients, were significant.

Table 4. Results of Hydrodynamic Correlations

A) for $\left(\frac{U_{G_{mf}}}{U^{o}_{G_{mf}}}\right) = a\left(\frac{U_{L_{mf}}}{U^{o}_{L_{mf}}}\right)$

Type of Packing	a	b ± 1σ	c ± 1σ	Multiple Correlation Coefficient	F-Value
4x8 alumina	6.325×10^{-6}	-0.177 ± 0.328		0.187	0.290
8x12 alumina	4.445×10^{-8}	-0.248 ± 0.294		0.258	0.714
¼-in. Plexiglas	2.422×10^{-8}	-0.266 ± 0.416		0.208	0.408

B) for $\varepsilon_S = a\left(\frac{U_L}{U_{L_{mf}}}\right)^{b}(U_G)^{c}$

4x8 alumina	0.559	-0.020 ± 0.012	0.001 ± 0.0004	0.544	9.265
8x12 alumina	0.629	-0.205 ± 0.017	0.004 ± 0.008	0.883	68.795
¼-in. Plexiglas	0.455	-0.196 ± 0.050	-0.014 ± 0.042	0.480	8.078
3 sets of data combined	0.509	-0.076 ± 0.020	0.002 ± 0.002	0.304	7.283

The correlations found for the solid volume fraction relations are:

$$\varepsilon_{S(4x8\ alumina)} = 0.559\ \left(\frac{U_L}{U_{L_{mf}}}\right)^{-0.02\pm0.012}$$

$$\varepsilon_{S(8x12\ alumina)} = 0.629\ \left(\frac{U_L}{U_{L_{mf}}}\right)^{-0.205\pm0.017}$$

$$\varepsilon_{S(0.25\text{-in. Plexiglas})} = 0.455\left(\frac{U_L}{U_{L_{mf}}}\right)^{-0.196\pm0.050}$$

$$\varepsilon_{S(combined)} = 0.509\left(\frac{U_L}{U_{L_{mf}}}\right)^{-0.076\pm0.020}$$

For the above cases the confidence level exceeded 99.9%. The solid volume fraction dependence on the superficial gas velocity was eliminated, since the regression coefficients were neither significant nor justified with standard deviations equal to or greater than the coefficient. The independence of the solid volume fraction of the superficial gas velocity contradicts the findings of Saad et al. (1) which were based on a limited number of runs at a lower bed height. Saad et al. found a significant dependence of the solid volume fraction on superficial gas velocity.

4.1.7 Independent Determination of Liquid Volume Fraction

In previous studies the liquid volume fraction has been determined as the residual after the other experimentally determined fractions have been subtracted from one [Eq. (3)]. The compounded effect of errors in the gas and solid volume fractions on the liquid volume fraction should be eliminated by determining the liquid volume fraction independently of the other fractions. Two methods are proposed: tracer response measurements or solution of a set of simultaneous equations describing the system.

The tracer technique involves monitoring the column outlet for detectable materials at constant fluid velocity after the material has been injected into the column. A concentration profile may be plotted against time, and a mean concentration and residence time may be determined. Multiplying the volumetric flow rate by the mean residence time yields the average liquid volume holdup. The material injected might be a dye or ionic solution whose concentration is detected by a spectrophotometer or conductivity meter, respectively.

The second method, only applicable to fluidized beds, involves solving two simultaneous equations:

$$\varepsilon_L + \varepsilon_S + \varepsilon_G = 1.0$$

$$\Delta P = (\varepsilon_L \rho_L + \varepsilon_S \rho_S + \varepsilon_G \rho_G) H$$

The solid volume fraction is accurately determined by Eq. (12). All values except the gas and liquid volume fractions are known or determined by experimentation. Solving the above two equations for the gas and liquid volume fractions yields:

$$\varepsilon_G = \frac{\rho_L - \varepsilon_S \rho_L - \frac{\Delta P}{H} + \varepsilon_S \rho_S}{\rho_L - \rho_G} \tag{13}$$

$$\varepsilon_L = 1.0 - \varepsilon_S - \frac{\rho_L - \varepsilon_S \rho_L - \frac{\Delta P}{H} + \varepsilon_S \rho_S}{\rho_L - \rho_G} \tag{14}$$

This method would require accurate determinations of both bed height (see Appendix 8.1) and pressure drop through the bed. A second manometer should be attached at the top of the bed and its height compared to the current manometer so that the pressure drop in the bed can be calculated without the interference of the bubble column region. A glass or rigid, clear plastic tube inside the column with a J-shaped end to prevent the entrance of gas bubbles can be used if the tip is small enough to prevent the entry of packing particles. Since the manometer level will usually be below that in the column, a small layer of colored oil at the top of the manometer would make the liquid height much easier to measure. If the tube is small and is kept against the column wall, there should be little disruption of flow or dispersion.

4.1.8 Future Work on Hydrodynamics

Although an objective of the hydrodynamics study was to define the various phase volume fractions as a function of the superficial velocities, particle diameter, density, and shape factor so that the fluidization behavior at particular operating conditions can be predicted, the scatter of data for the effect of flow velocities on gas volume fraction was so large that only one valid correlation could be derived. Therefore, the recomendations for further work in hydrodynamics are:

1. Eliminate or quantify the sources of error in gas volume fraction measurements.

2. Determine the liquid volume fraction independently as proposed in the previous section since the increased uncertainties associated with measurement of gas and solid volume fractions give inaccurate determination

of liquid volume fraction as the difference of gas and liquid volume fractions from one.

3. Test Eq. (10) against the data once accurate correlations of volume fractions as a function of the above parameters are derived.

4. Use packed bed correlations for the regime prior to fluidization.

5. Perform a dimensional analysis to determine

$$F\left(\varepsilon_G, \varepsilon_L, \varepsilon_S, \phi_S, \frac{\Delta P}{\varepsilon_S[\rho_S - (\varepsilon_G'\rho_G + \varepsilon_L'\rho_L)]H}, \frac{U_L}{U_G}, Re = \frac{D_p U_G \rho_L}{\mu_L}, \frac{D_p}{H}\right) = 0 \tag{15}$$

These parameters may be correlated to include various forces influencing the fluidization behavior, including the inertial forces represented by the Reynolds number and the drag and gravitational forces. Several correlations of interest are:

$$\frac{\Delta P}{\varepsilon_S[\rho_S - (\varepsilon_G'\rho_G + \varepsilon_L'\rho_L)]H} = f\left(\frac{U_L}{U_G}\right) \tag{16}$$

$$\varepsilon_G = f(Re, \phi_S) \tag{17}$$

$$\varepsilon_L = f(Re, \phi_S) \tag{18}$$

4.2 Mass Transfer

4.2.1 Experimental Conditions

Mass transfer experiments were completed for two types of packings: a 40-cm column of 0.25-in. Plexiglas spheres and a 48-cm column of 4x8 mesh alumina beads and a bubble column. The choice of operating conditions for the experiments was given in Sect. 3.3. These operating conditions are listed in Table 5. Run Nos. 18, 20, and 21 from Saad et al.(1) are included for comparison. The extraction factor, F, which characterizes the operating conditions is defined as

$$F = m_{exp}\left(\frac{U_L}{U_G}\right)$$

Table 5. Summary of Mass Transfer Experiments

Run No.	Type of Packing	U_L (cm/sec)	U_G (cm/sec)	m_{exp}	m_{lit}	% Error in m_{exp} $\left(\frac{m_{lit} - m_{exp}}{m_{lit}}\right)$	F $m_{exp}\left(\frac{U_L}{U_G}\right)$
A*	¼-in. Plexiglas	0.884	1.67	0.746	0.885	+15.7	0.395
B	¼-in. Plexiglas	2.14	4.05	0.954	0.865	-10.3	0.504
C	bubble column	2.14	4.05	0.901	0.800	-12.6	0.476
D	¼-in. Plexiglas	3.39	6.45	0.987	0.894	-10.4	0.519
E*	4x8 mesh alumina	3.39	6.45	0.839	0.87[illegible]	+ 4.2	0.441
F	bubble column	3.02	6.45	1.093	0.889	-22.9	0.512
G	4x8 mesh alumina	4.63	8.80	0.856	0.815	- 5.0	0.450
						avg 11.6	
Saad 18	4x8 mesh alumina	3.12	12.1	0.979	0.898	- 9.0	0.253
Saad 20	4x8 mesh alumina	5.48	11.7	1.216	0.910	-33.6	0.572
Saad 21	4x8 mesh alumina	5.48	11.6	1.237	0.922	-34.2	0.584

*Incipient fluidization

where m_{exp} is the experimental Henry's Law constant and is included in Table 5. The literature value of Henry's Law constant, m_{lit}, is also included in Table 5 and can be compared to the experimental values. In Runs 20 and 21 of Saad et al. (1), the experimental and literature values of Henry's Law constant differed by more than 30% which makes the validity of these runs questionable. Run F of this study is also questionable because of the 23% deviation in Henry's Law constant.

In Runs E and G in which 4x8 mesh alumina packing was used, an equilibrium determination could not be made because the packing slowly disintegrated and released acidic silicates into the liquid and continually changed the column pH. The equilibrium data to obtain the Henry's Law constant for Runs E and G were taken from Run C which had approximately the same column temperature.

4.2.2 Column Concentration Profiles

Plots of the experimental concentration profile, X, and the dimensionless column height, Z, are presented in Figs. 7 through 16. The fractional approach to equilibrium, X, is defined as:

$$X = \frac{mC_{G_{in}} - C_L}{mC_{G_{in}} - C_{L_{in}}} \tag{19}$$

and the dimensionless column height, Z, is defined as:

$$Z = \frac{h_{\text{sample port}}}{h_{\text{top port}}} \tag{20}$$

For each mass transfer experiment a theoretical column concentration profile was obtained using a dispersed liquid and gas plug flow model (1). These theoretical profiles are drawn in the figures. The experimental fractional approach to equilibrium obtained at the top of the bed was used to calculate an overall mass transfer coefficient from the dispersion model with an assumed dispersion coefficient. A theoretical column concentration profile was then obtained from this overall mass transfer coefficient. The value of the dispersion coefficient that best fit the model to the data was selected by trial and error. The computer program used in this procedure is presented in Appendix 8.6.

In Runs B and C and Saad's Run 21, the value of the fractional approach to equilibrium at the top port deviated from the remainder of the data. For these runs the fractional approach to equilibrium at the outlet used in the theoretical concentration profile was obtained by extrapolating the plot of the experimental fractional approach to equilibrium as a function

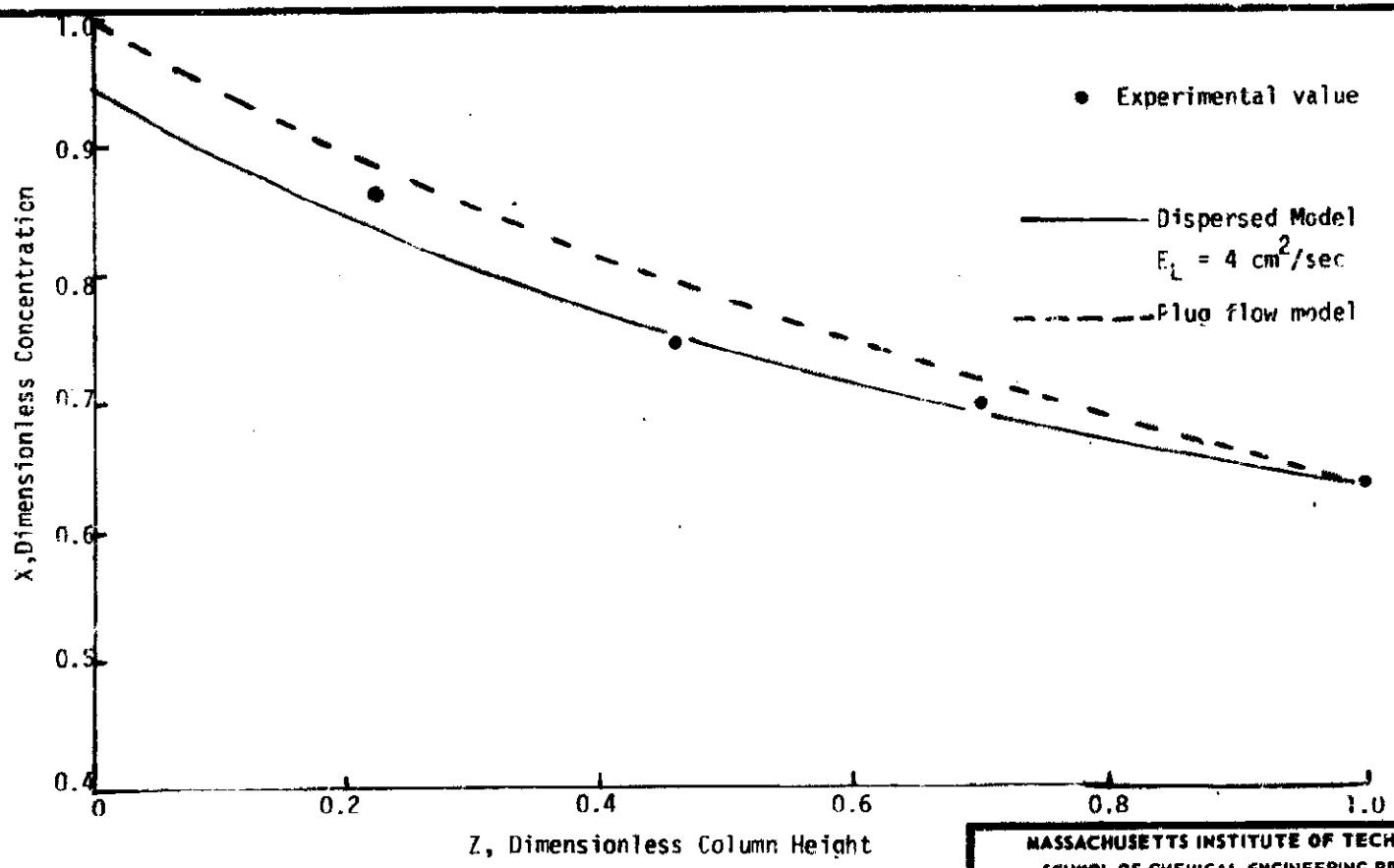

Packing: 0.25-in. Plexiglas spheres

U_L = 0.884 cm/sec

U_G = 1.67 cm/sec

MASSACHUSETTS INSTITUTE OF TECHNOLOGY
SCHOOL OF CHEMICAL ENGINEERING PRACTICE
AT
OAK RIDGE NATIONAL LABORATORY

CONCENTRATION PROFILE FOR RUN A

DATE	DRAWN BY	FILE NO.	FIG.
5-19-75	RM	CEPS-X-213	7

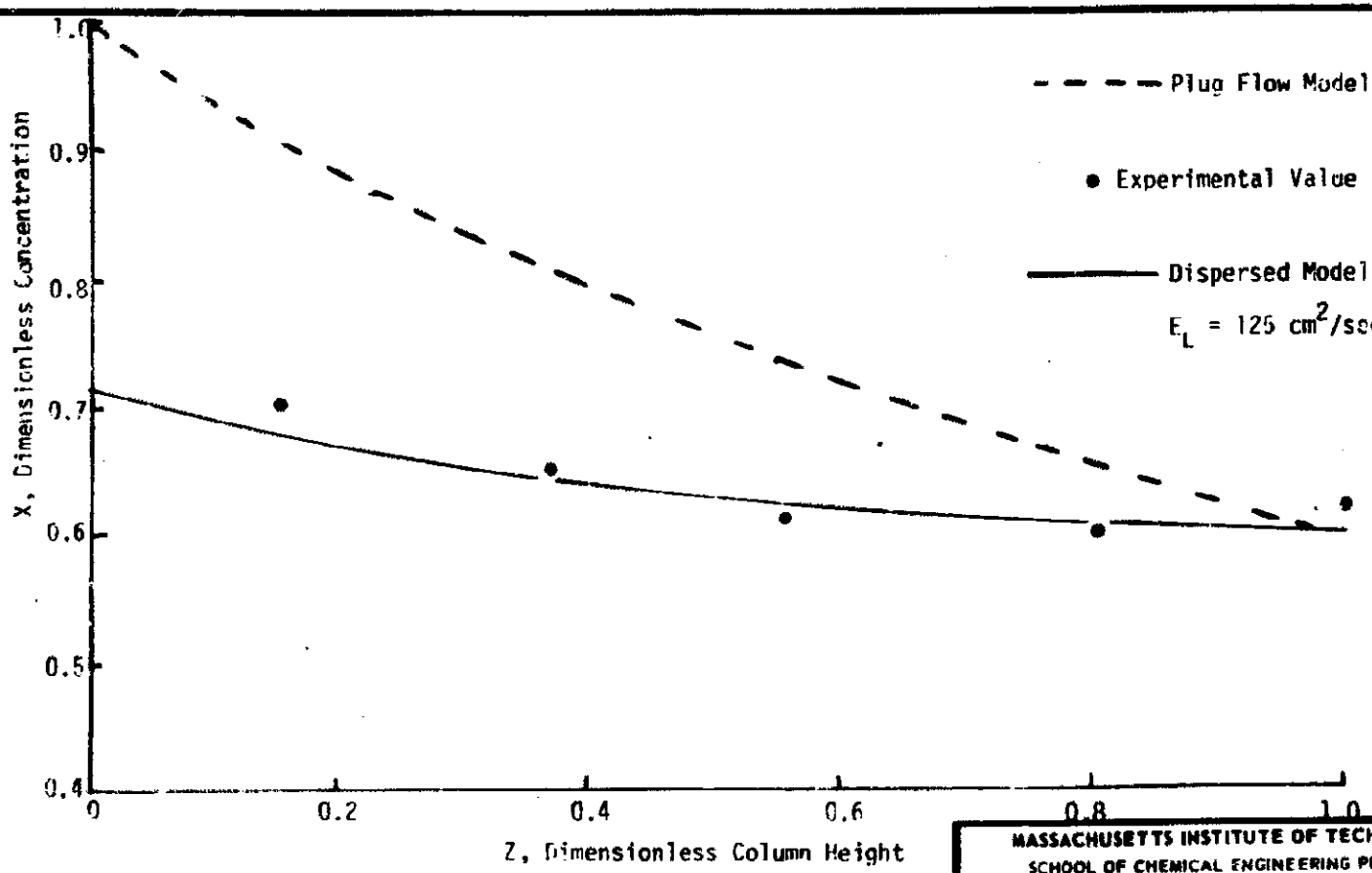

Packing: 0.25-in. Plexiglas spheres

U_L = 2.14 cm/sec

U_G = 4.05 cm/sec

MASSACHUSETTS INSTITUTE OF TECHNOLOGY
SCHOOL OF CHEMICAL ENGINEERING PRACTICE
AT
OAK RIDGE NATIONAL LABORATORY

CONCENTRATION PROFILE FOR RUN B

DATE	DRAWN BY	FILE NO.	FIG.
5-19-75	RM	CEPS-X-213	8

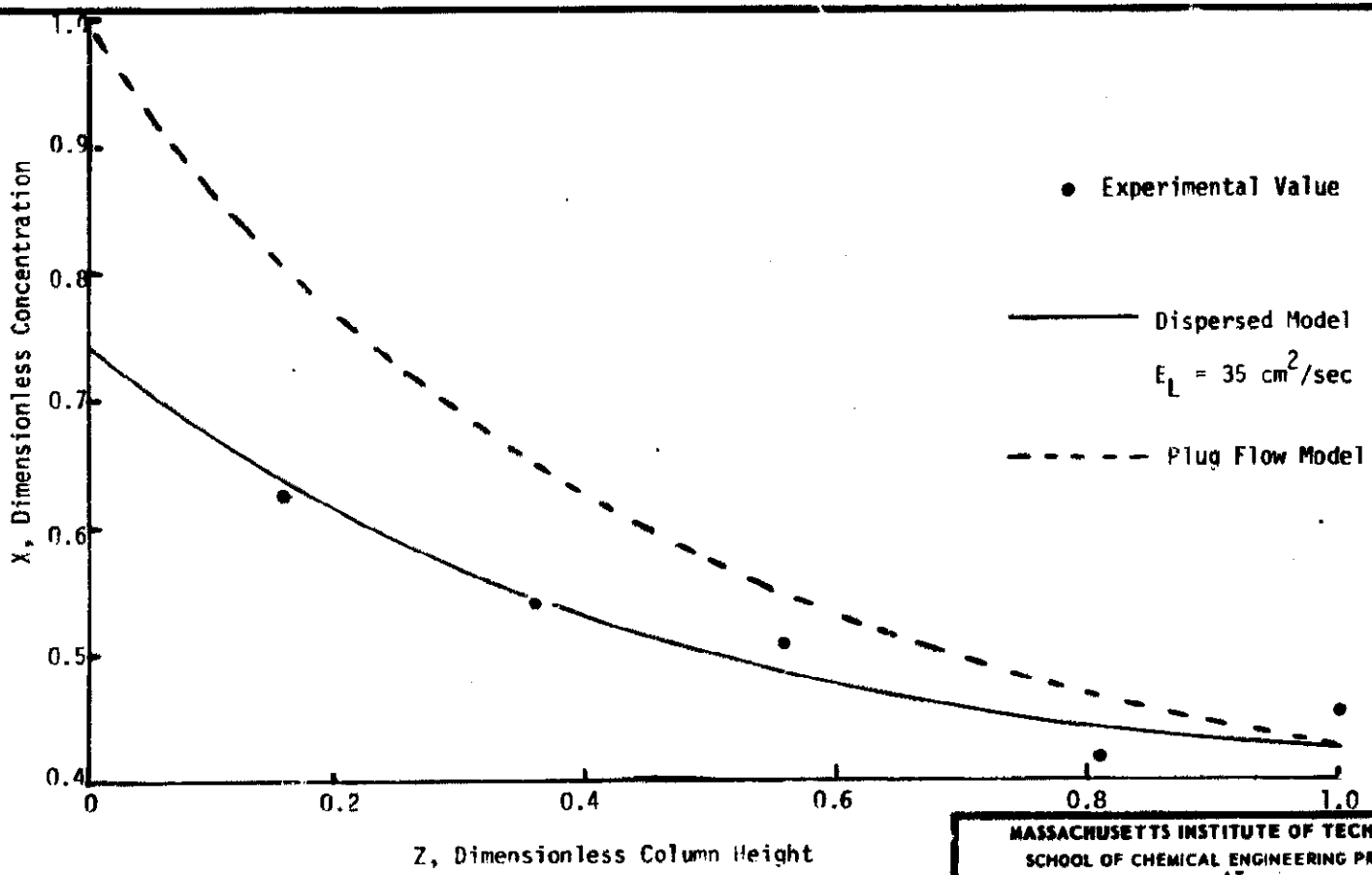

Bubble Column

U_L = 2.14 cm/sec

U_G = 4.05 cm/sec

MASSACHUSETTS INSTITUTE OF TECHNOLOGY
SCHOOL OF CHEMICAL ENGINEERING PRACTICE
AT
OAK RIDGE NATIONAL LABORATORY

CONCENTRATION PROFILE FOR RUN C

DATE	DRAWN BY	FILE NO	FIG.
5-19-75	RM	CEPS-X-213	9

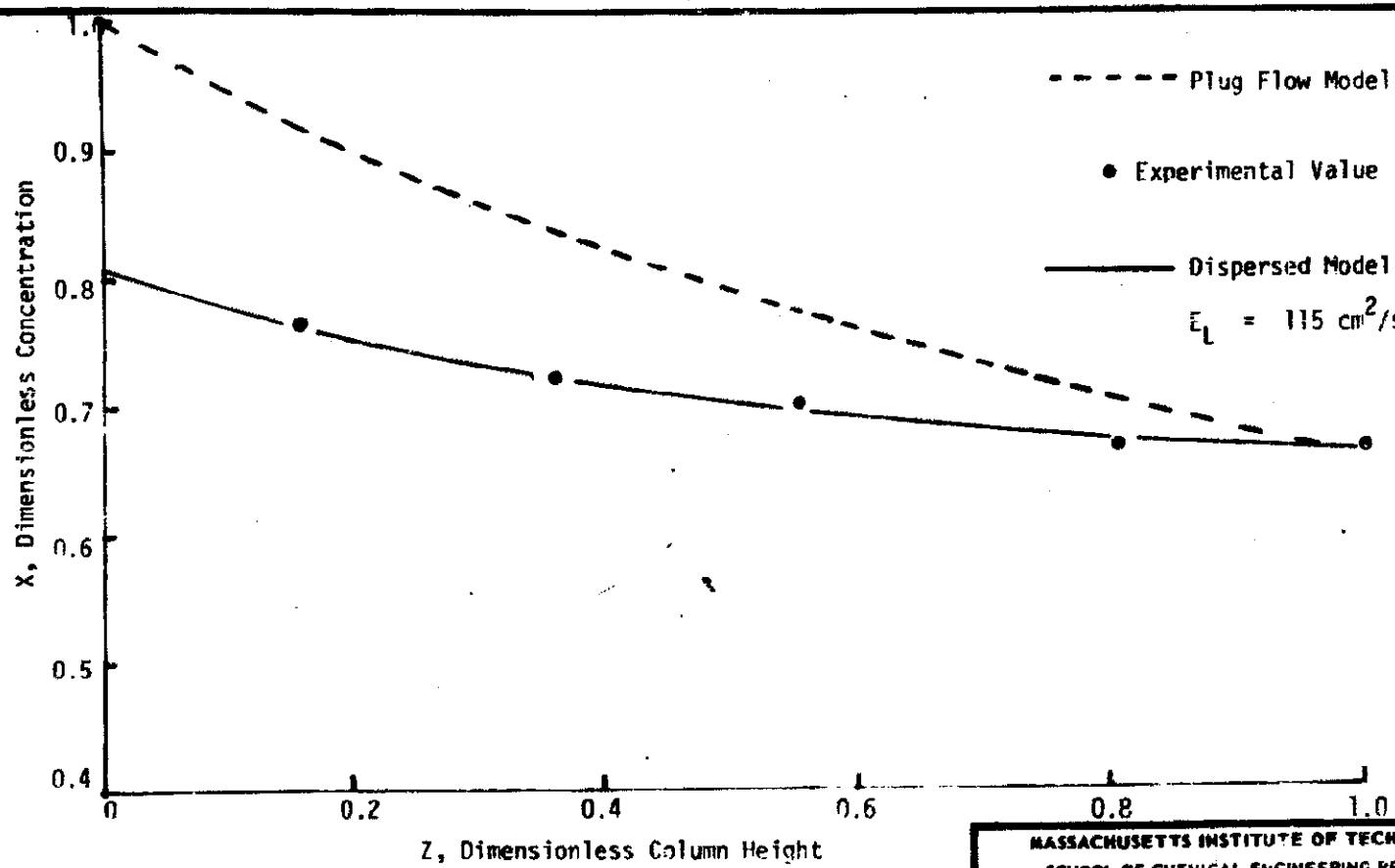

Packing: 0.25-in. Plexiglas spheres

U_L = 3.39 cm/sec

U_G = 6.45 cm/sec

MASSACHUSETTS INSTITUTE OF TECHNOLOGY
SCHOOL OF CHEMICAL ENGINEERING PRACTICE
AT
OAK RIDGE NATIONAL LABORATORY

CONCENTRATION PROFILE FOR RUN D

DATE	DRAWN BY	FILE NO.	FIG.
5-19-75	RM	CEPS-X-213	10

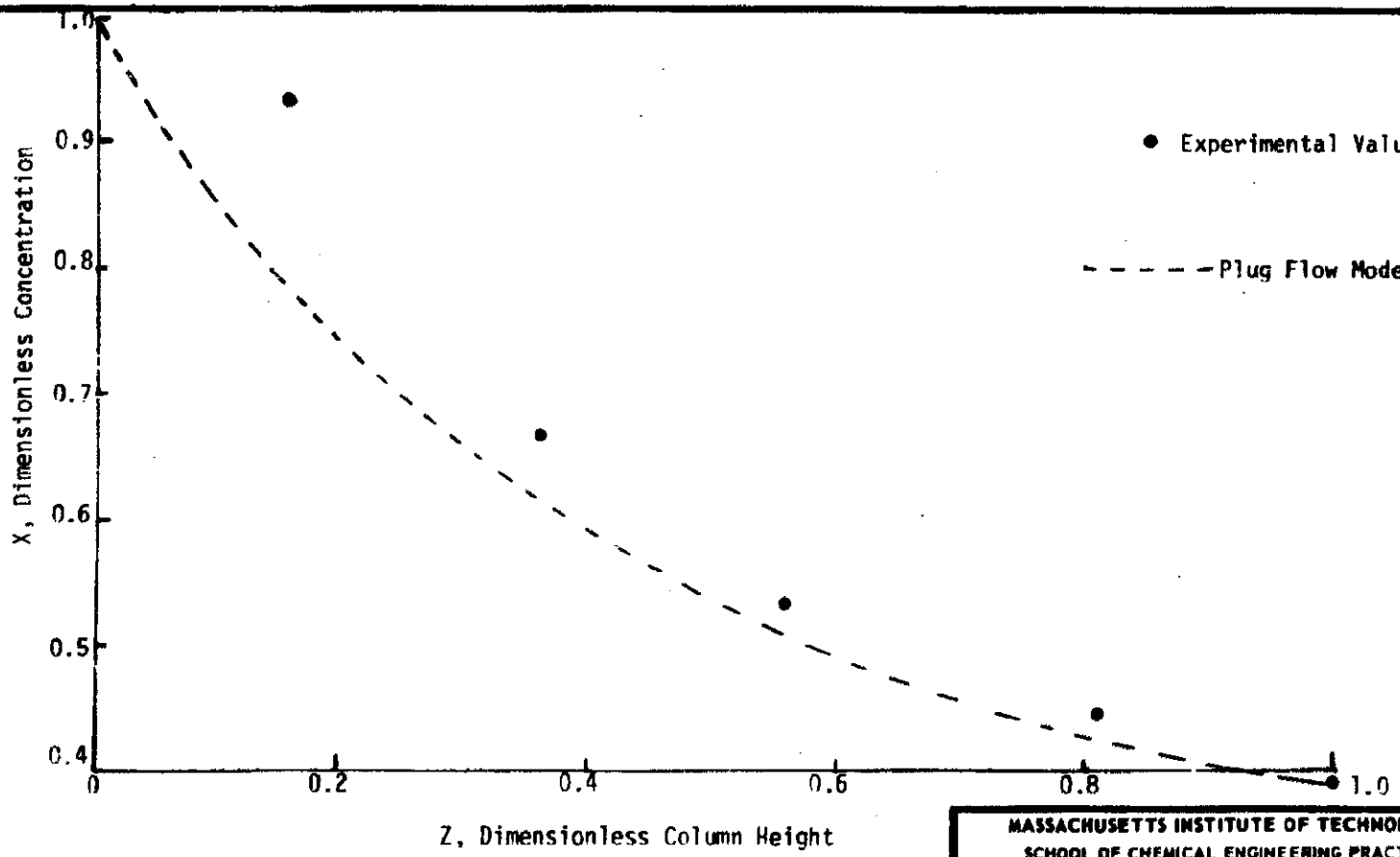

Packing: 4x8 Mesh Alumina

U_L = 3.39 cm/sec

U_G = 0.45 cm/sec

MASSACHUSETTS INSTITUTE OF TECHNOLOGY
SCHOOL OF CHEMICAL ENGINEERING PRACTICE
AT
OAK RIDGE NATIONAL LABORATORY

CONCENTRATION PROFILE FOR RUN E

DATE	DRAWN BY	FILE NO.	FIG.
5-19-75	RM	CEPS-X-213	11

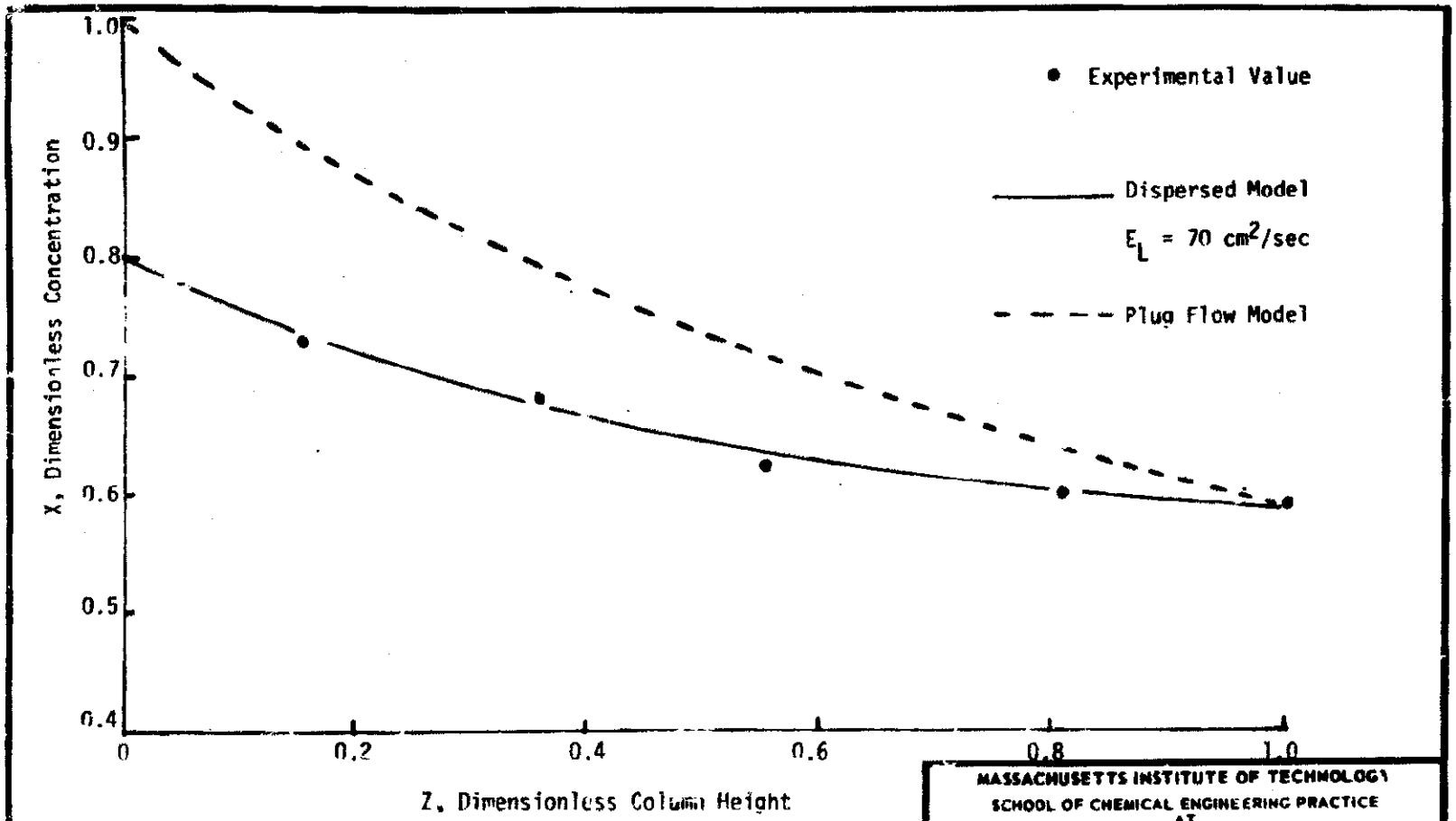

Bubble Column

U_L = 3.02 cm/sec

U_G = 6.45 cm/sec

MASSACHUSETTS INSTITUTE OF TECHNOLOGY
SCHOOL OF CHEMICAL ENGINEERING PRACTICE
AT
OAK RIDGE NATIONAL LABORATORY

CONCENTRATION PROFILE FOR RUN F

DATE	DRAWN BY	FILE NO.	FIG.
5-19-75	RM	CEPS-X-213	12

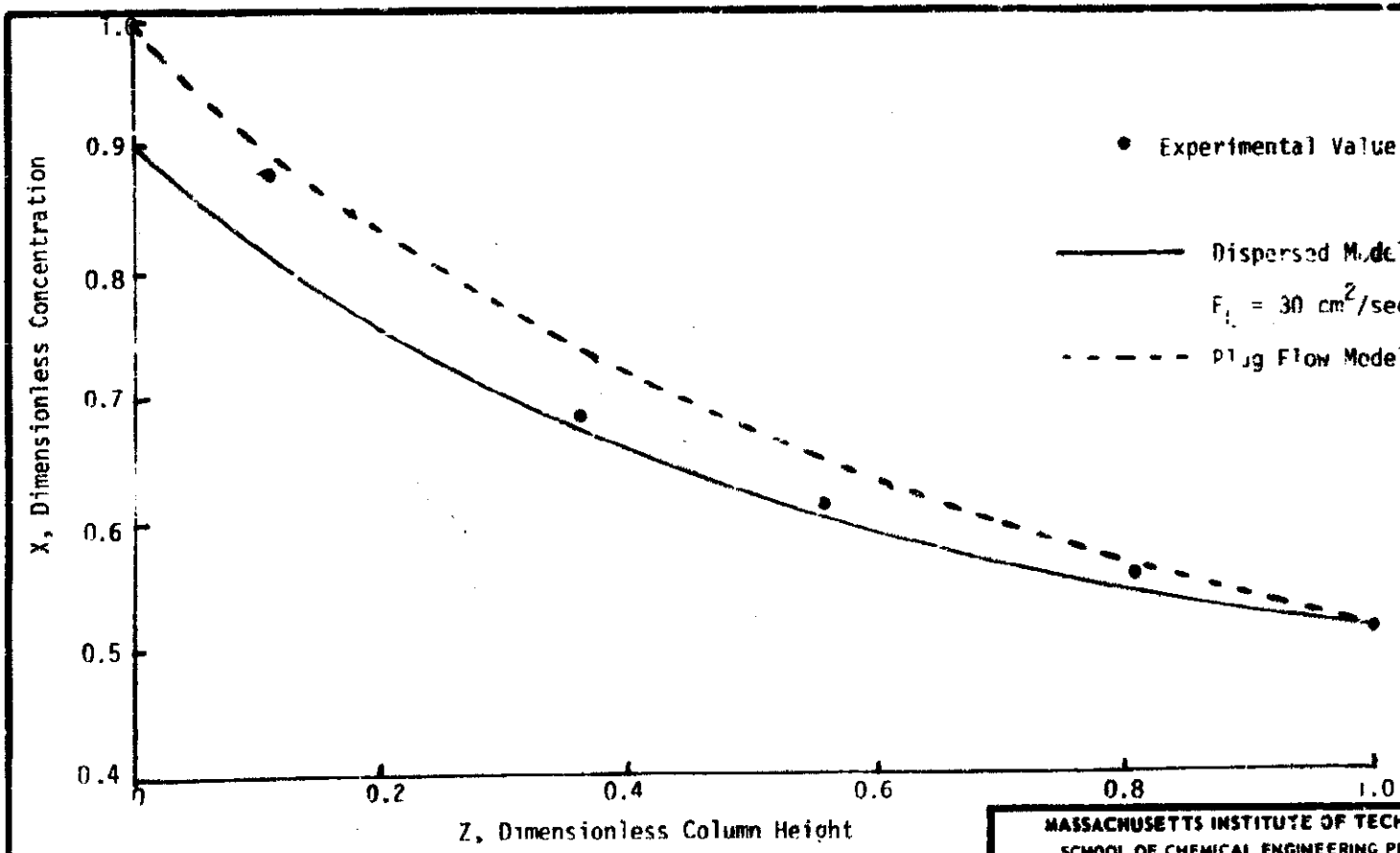

Packing: 4x8 Mesh Alumina Beads

U_L = 4.63 cm/sec

U_G = 8.86 cm/sec

MASSACHUSETTS INSTITUTE OF TECHNOLOGY
SCHOOL OF CHEMICAL ENGINEERING PRACTICE
AT
OAK RIDGE NATIONAL LABORATORY

CONCENTRATION PROFILE FOR RUN G

DATE	DRAWN BY	FILE NO.	FIG.
5-19-75	RM	CEPS-X-213	13

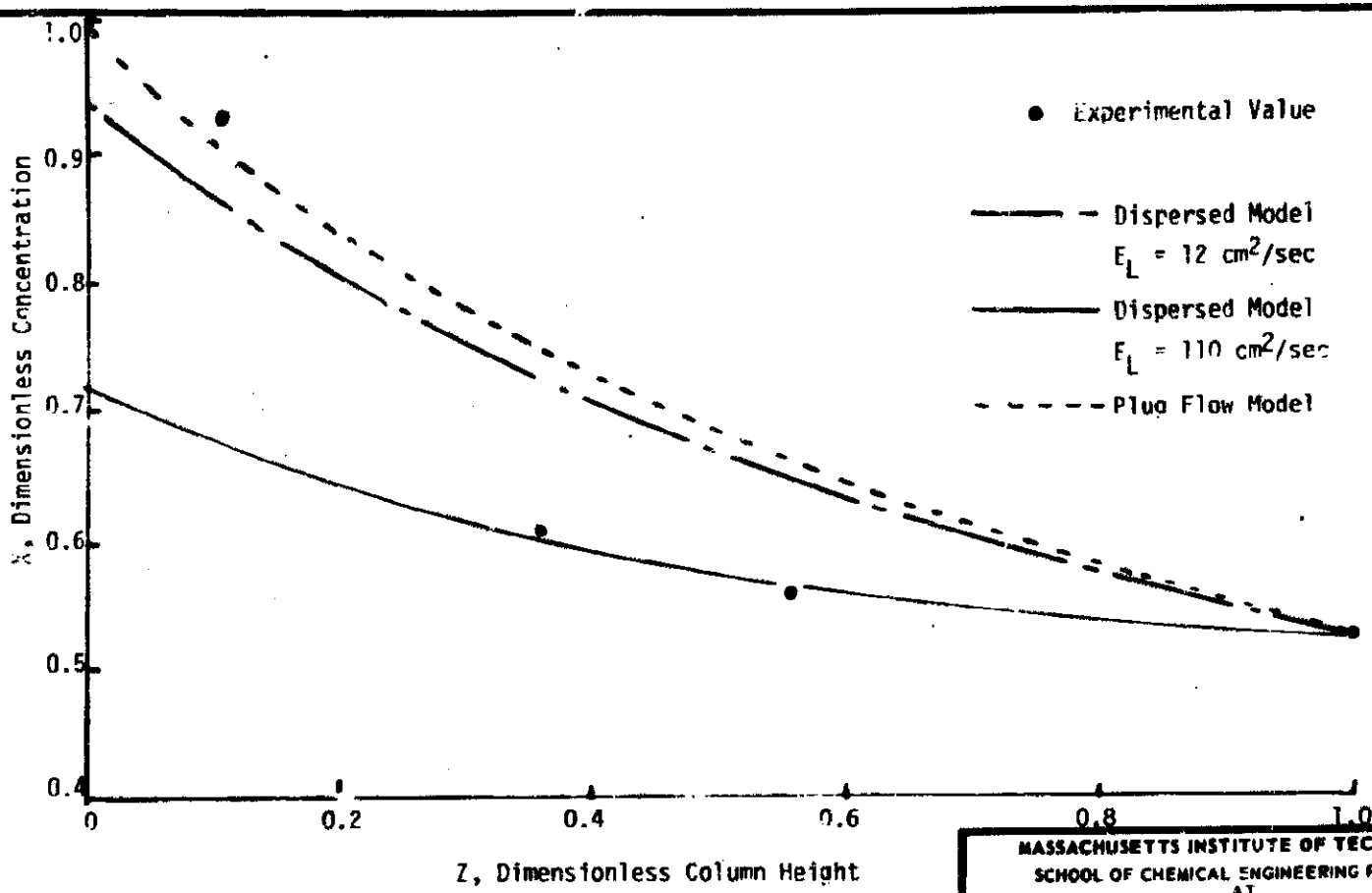

Packing: 4x8 Mesh Alumina Beads

U_L = 3.12 cm/sec

U_G = 12.1 cm/sec

MASSACHUSETTS INSTITUTE OF TECHNOLOGY
SCHOOL OF CHEMICAL ENGINEERING PRACTICE
AT
OAK RIDGE NATIONAL LABORATORY

CONCENTRATION PROFILE FOR SAAD RUN 18

DATE	DRAWN BY	FILE NO.	FIG.
5-19-75	RM	CEPS-X-213	14

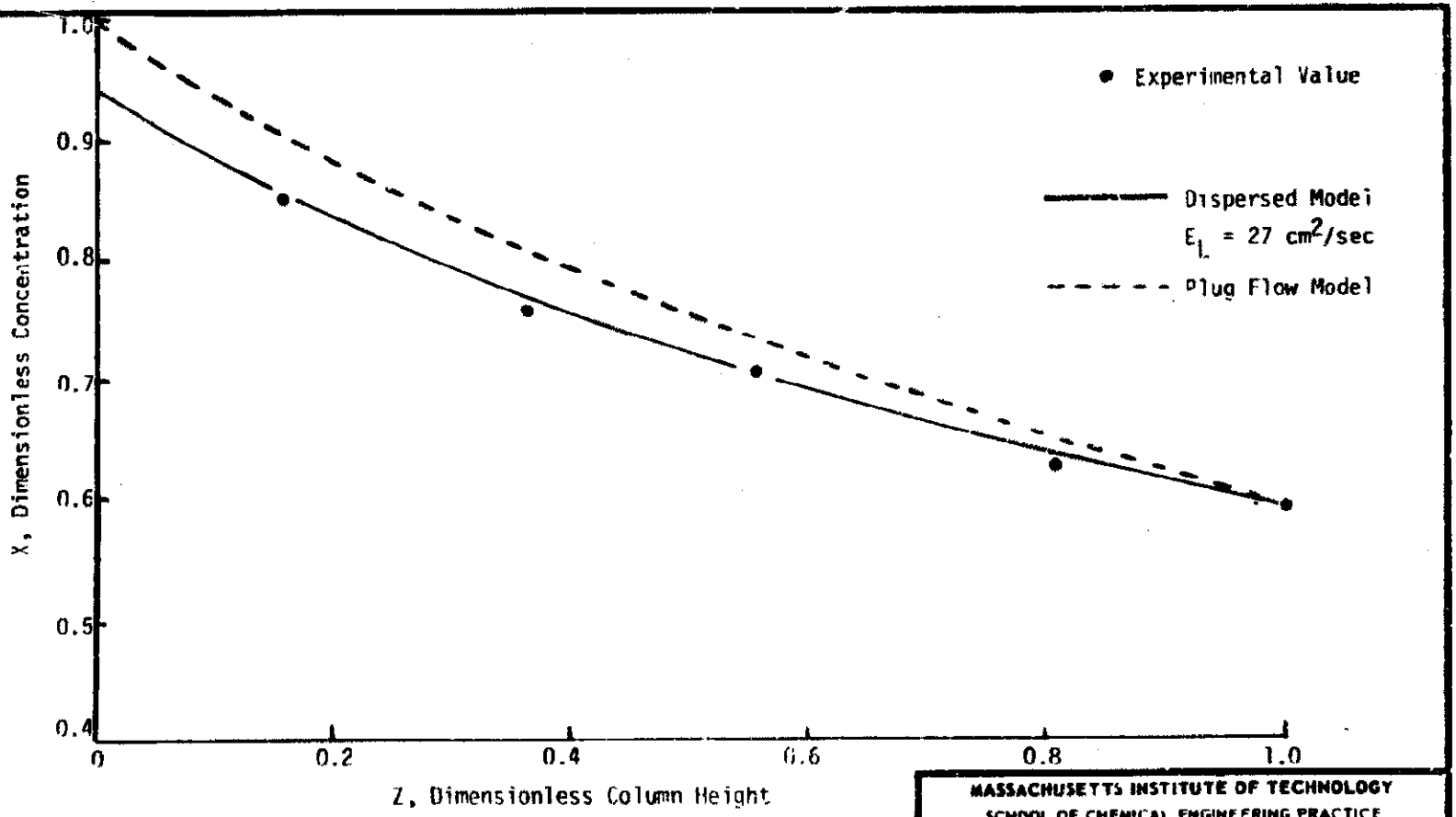

Packing: 4x8 Mesh Alumina Beads

U_L = 5.48 cm/sec

U_G = 11.7 cm/sec

MASSACHUSETTS INSTITUTE OF TECHNOLOGY
SCHOOL OF CHEMICAL ENGINEERING PRACTICE
AT
OAK RIDGE NATIONAL LABORATORY

CONCENTRATION PROFILE FOR SAAD RUN 20

DATE	DRAWN BY	FILE NO.	FIG.
5-14-75	RM	CEPS-X-213	15

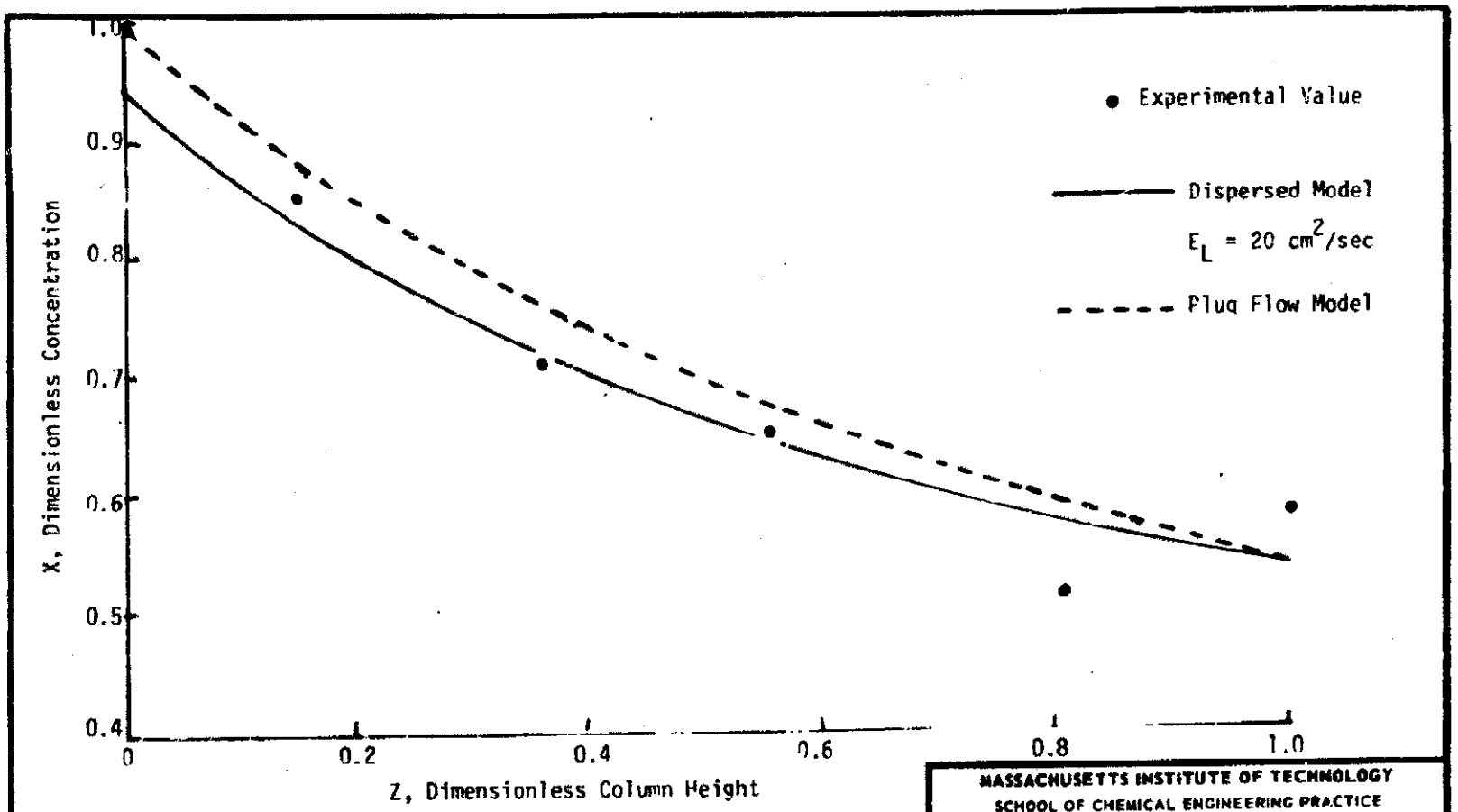

Packing: 4x8 Mesh Alumina Beads

U_L = 5.48 cm/sec

U_G = 11.6 cm/sec

MASSACHUSETTS INSTITUTE OF TECHNOLOGY
SCHOOL OF CHEMICAL ENGINEERING PRACTICE
AT
OAK RIDGE NATIONAL LABORATORY

CONCENTRATION PROFILE FOR SAAD RUN 21

DATE	DRAWN BY	FILE NO.	FIG.
5-19-75	RM	CEPS-X-213	16

of dimensionless bed height. The concentration profiles for runs of Saad et al. (1) are based on a column height from the liquid rather than the gas distributor which Saad used as explained in Sect. 8.4.1.

The dispersed liquid flow model approaches a plug flow model at low values of the dispersion coefficient and a well-mixed (CSTR) model at high values of the dispersion coefficient (1). For the Plexiglas runs, as the liquid and gas flow rates increased, the flow pattern changed from approximately plug flow to CSTR flow. In the alumina runs, Figs. 11 and 13 to 16, the liquid flow pattern deviated much less from plug flow than in the Plexiglas runs for similarly fluidized conditions.

In Table 6 the operating conditions, dispersion coefficient, and overall mass transfer coefficient are summarized for each run. The average dispersion coefficient for the Plexiglas runs was 81 cm^2/sec compared to 37 cm^2/sec for the alumina runs. Runs D and E with Plexiglas and alumina, respectively, were conducted at identical operating conditions. The dispersion coefficients were 115 and 0 cm^2/sec, respectively.

Table 6. Summary of Dispersion Coefficients and Overall Mass Transfer Coefficients

Run	Packing	U_L (cm/sec)	U_G (cm/sec)	E (cm^2/sec)	K_La (sec^{-1})
A	¼-in. Plexiglas	0.884	1.67	4	0.0124
B	¼-in. Plexiglas	2.14	4.05	125	0.0342
C	bubble column	2.14	4.05	35	0.0736
D	¼-in. Plexiglas	3.39	6.45	115	0.0384
E	4x8 mesh alumina	3.39	6.45	0	0.109
F	bubble column	3.02	6.45	70	0.0480
G	4x8 mesh alumina	4.63	8.80	30	0.0894
Saad 18	4x8 mesh alumina	3.12	12.1	110	0.0595
Saad 20	4x8 mesh alumina	5.48	11.7	27	0.0773
Saad 21	4x8 mesh alumina	5.48	11.6	20	0.0993

The average dispersion coefficient for the bubble column runs was 52 cm^2/sec. For Run C in Fig. 9, a value of 0.43 was used for the fractional approach to equilibrium at the top of the column to obtain a dispersion coefficient of 35 cm^2/sec. The value of the dispersion coefficient, however, was very sensitive to the value of the fractional approach to equilibrium at the column top. When the value (0.45) of the experimental point at Z=1 was used from Fig. 9 rather than the value of 0.43 obtained from the extrapolated curve, a dispersion coefficient of 55 cm^2/sec was found.

Experimental bubble column dispersion coefficients were compared to previous correlations (3). For Run C a literature value of the dispersion coefficient for countercurrent flow was found to be 84 cm^2/sec (see Appendix 8.3). This value is higher than the experimental values for cocurrent flow, which ranged between 35 and 55 cm^2/sec. For Run F the literature value of the dispersion coefficient was found to be 72 cm^2/sec compared to the experimental value of 70 cm^2/sec. Although the experimental and reported values of Henry's Law constant differed by 23%, the dispersion coefficient was found to be quite insensitive to changes in Henry's Law constant. A 25% change in the value of Henry's Law constant changed the dispersion coefficient by 3 to 5%.

In Run F the experimental values for the fractional approach to equilibrium as a function of dimensionless height formed a smooth curve with few deviations from the dispersed model. In Run C the values of the fractional approach to equilibrium at the top of the column deviated from the rest of the data. The dispersion coefficient was more sensitive to the fractional approach to equilibrium at the top of the column than to variations in Henry's Law constant. Better agreement between the reported and experimental values of the dispersion coefficient in Run F than in Run C is due to the more consistent data of Run F.

4.2.3 Overall Mass Transfer Coefficients

For 4x8 alumina and ¼-in. Plexiglas packing and an open bubble column, a plot of overall mass transfer coefficients is presented as a function of superficial gas velocity in Fig. 17. For a constant superficial gas velocity, the calculated overall mass transfer coefficients decreased in the following order: 4x8 mesh alumina packing, bubble column, and ¼-in. Plexiglas packing.

The overall mass transfer coefficients for the Plexiglas packing increase to 0.035 sec^{-1} at a superficial gas velocity of 4 cm/sec where they remained approximately independent of gas velocity. In Run A the liquid superficial velocity of 2 cm/sec was just below incipient fluidization. Based on two data points, the overall mass transfer coefficients obtained for the bubble column decrease in magnitude with increasing gas velocity. At the superficial gas velocity of 4.1 cm/sec, the experimental concentration profile was not very consistent as explained in Sect. 4.2.2 and introduced an error of more than 10% in the overall mass transfer coefficient. For the overall mass transfer coefficient at a superficial gas velocity of 6.5 cm/sec, the experimental Henry's Law constant was 23% higher than the literature value. In both cases the errors would tend to decrease the overall mass transfer coefficients in Fig. 17.

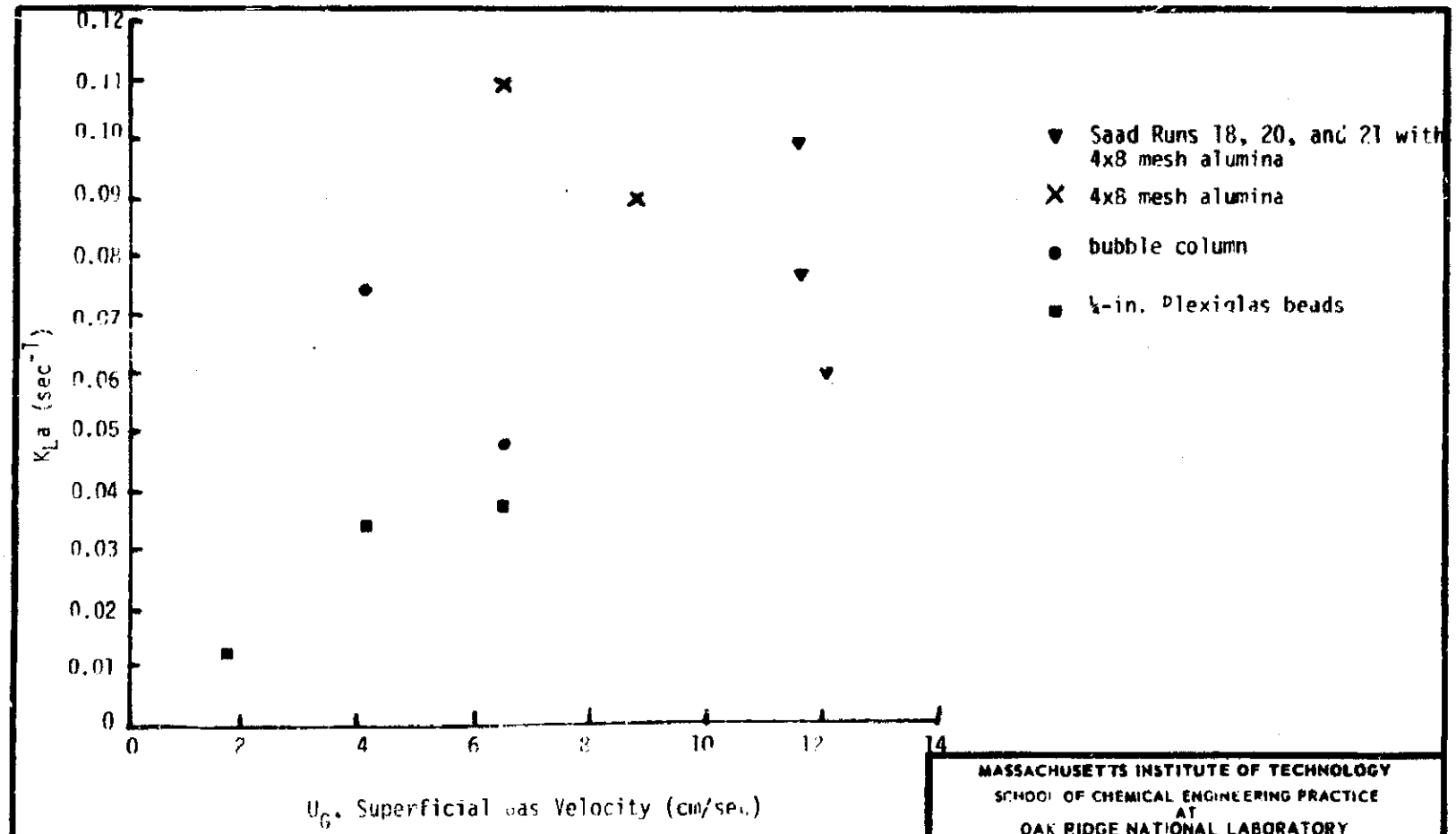

MASSACHUSETTS INSTITUTE OF TECHNOLOGY
SCHOOL OF CHEMICAL ENGINEERING PRACTICE
AT
OAK RIDGE NATIONAL LABORATORY

OVERALL MASS TRANSFER COEFFICIENT FOR VARIOUS PACKINGS AS A FUNCTION OF SUPERFICIAL GAS VELOCITY

DATE	DRAWN BY	FILE NO.	FIG.
5-19-75	RM	CEPS-X-213	17

Run 18 of Saad et al. (1) for the 4x8 mesh alumina and a superficial gas velocity of 12.1 cm/sec had a packed bed height of 13 cm and top sample port at 48 cm. The overall mass transfer coefficient was in the range of the overall mass transfer coefficient for the bubble column runs because, with the low bed height, the column was in effect a bubble column. In addition, the dispersion coefficient of 110 cm^2/sec was similar to the dispersion coefficients of 35 and 70 cm^2/sec for the other bubble column runs. The other overall mass transfer coefficients for the 4x8 alumina packing were scattered between 0.0773 and 0.109 sec^{-1} and generally appeared to decrease with increasing gas velocity. Runs 20 and 21 of Saad et al. had experimental values of Henry's Law constant which were over 30% greater than the corresponding reported values. With this deviation, the overall mass transfer coefficients for these runs may be 10% lower than those plotted in Fig. 17.

Michelson and Ostergaard (2) have noted that for particles of similar density (2.6 gm/cc), large particles (6 mm) increase and small ones (1 mm) decrease the overall mass transfer coefficient compared to that found in a bubble column for similar flow conditions. The ¼-in. (6.4 mm), 1.9-gm/cc alumina beads currently used also increased the overall mass transfer coefficient. In addition, the less dense (¼-in., 1.2 gm/cc) particles as well as smaller (1 mm, 2.6 gm/cc) particles lower the overall mass transfer coefficient.

An extrapolation of the dispersion coefficient plot of Michelson and Ostergaard (2) into the low flow region currently studied gives values which generally agree with the dispersion coefficients found for ¼-in. alumina beads. A quantitative correlation of solid density effects will require more accurate liquid volume fraction data.

5. CONCLUSIONS

1. Liquid volume fractions may be better determined by accurate measurement of the bed pressure drop or by the use of tracers such as dyes or ionic solutions.

2. An increase in the superficial gas velocity decreases the superficial minimum liquid fluidization velocity. However, the minimum liquid fluidization velocity quickly becomes independent of the superficial gas velocity for superficial gas velocities of 1 to 4 cm/sec.

3. Increases in packed bed height lowered the minimum liquid fluidization velocity.

4. The solid volume fraction remains constant with increasing gas and liquid velocities until the point of incipient fluidization, where the slope of solid volume fraction as a function of liquid velocity shows a distinct change. The following correlation was derived based on data for three packings.

$$\varepsilon_S = 0.509\left(\frac{U_L}{U_{Lmf}}\right)^{-0.076\pm0.020}$$

5. The gas volume fraction data were too scattered for a correlation to be significant.

6. As the solid density increased, the solid and gas volume fractions increased while the liquid fraction decreased.

7. The experimental techniques for measuring pressure drop, bed height, and the phase volume fractions should be improved.

8. The dispersion coefficient (120 cm^2/sec) for ¼-in. Plexiglas spheres is greater by a factor of three than for a bubble column at similar flow rates. The overall mass transfer coefficient of 0.038 sec^{-1} for the same Plexiglas spheres is smaller by a factor of two at most.

9. The dispersion coefficient for 4x8 mesh alumina beads (30 cm^2/sec) is smaller than the coefficient for a bubble column with similar flows. The liquid flow is approximated as plug flow. The overall mass transfer coefficient of 0.09 sec^{-1} is larger than the bubble column coefficient by a factor of 1.5 to 2.

6. RECOMMENDATIONS

1. The following improvements in experimental techniques are suggested: (a) install a ball valve in the water drain line for gas volume fraction measurements, (b) measure the liquid volume fraction independently by a pressure drop or a tracer method, (c) use a moveable J-shape manometer in the column to measure the pressure at the top of the bed and more accurately determine the pressure drop across the bed, (d) develop a standard experimental method to determine the degree of fluidization, and (e) develop a standard method to determine the bed height (e.g., photograph determination of the region containing a fixed fraction of particles).

2. For the further study of hydrodynamics (a) better data should be obtained to test the correlations presented, (b) the existing literature correlations should be modified for two phase fluidized beds to include a third phase, and (c) further correlations should be developed by dimensional analysis.

3. For the further study of mass transfer (a) the bed height should be raised closer to the outlet to reduce the effect of backmixing from the bubble column region to the top of the bed and (b) the alumina beads should be replaced with an inert and non-brittle material so water can be cycled through the stripper at high flow rates without clogging the liquid disperser. Equilibrium can then be more accurately determined.

7. ACKNOWLEDGMENT

We express our gratitude to J.M. Begovich and J.S. Watson for their help during the course of the project.